CORRELATION BETWEEN fMRI and SOURCE RECONSTRUCTED EEG of STEADY STATE VISUAL EVOKED POTENTIALS

by

Hüseyin Hamdi Eryılmaz

B.S, in Electrical and Electronics Engineering, Middle East Technical University, 2004

Submitted to the Institute of Biomedical Engineering
in partial fulfillment of the requirements
for the degree of
Master of Science
in
Biomedical Engineering

Boğaziçi University
August 2007

ACKNOWLEDGMENTS

Firstly, I would like to thank my supervisor Prof. Ahmet Ademoğlu for his continuous support in preparation of this study. He has been a perfect thesis advisor in terms of directing my studies and projects. Another person who deserves high praise is my teammate Adil Deniz Duru. His help meant a lot to me during all the efforts to complete this thesis. I cannot forget to thank Burak Parlak, who also provided very important contribution and support. I also would like to thank Uzay Emrah Emir, Zübeyir Bayraktaroğlu and the members of the Physiology and Radiology departments of Istanbul University Medical Faculty who shared their experimental data with us. Besides, I appreciate the efforts of all the teammates in terms of providing help, data and moral support. I am also grateful to BAD (National Brain Research Association) for its funding support to our project. Finally, I cannot forget to thank my family, who continously supported me during my graduate education and did their best to provide all the encouragement I needed during the years.

ABSTRACT

CORRELATION BETWEEN fMRI and SOURCE RECONSTRUCTED EEG of STEADY STATE VISUAL EVOKED POTENTIALS

Electroencephalography (EEG) is a common technique for studying and understanding the functioning of the brain. In addition, functional Magnetic Resonance Imaging (fMRI), in the recent years has been a very conventional method for neuroimaging. The most important property of the EEG, which makes it superior to other neuroimaging modalities is its very high temporal resolution. EEG reflects functional activities in the range of milliseconds. However, due to limited number of electrode measurements and some modeling failures, it can provide limited spatial resolution. fMRI provides satisfactory spatial resolution for imaging of these processes but it lacks good temporal resolution. In this thesis, the steady state human visual evoked potentials and their corresponding fMRI scans are processed using EEG source reconstruction and fMRI statistical parametric mapping methods. The visual stimulations are ranging from 2 to 10 Hz. The fMRI voxels which proved significantly active were correlated with their associated EEG neuroelectric power which was determined on the same geometric head with Low Resolution Electromagnetic Tomography (LORETA). Spatially averaged positive BOLD, post-stimulus undershoot and LORETA amplitudes are determined across the frequencies as well as the spatial correlations between the positive BOLD and LORETA amplitudes over an activation mask. Finally, the correlation between the standardized regression parameter due to the steady state visual effect and the LORETA amplitudes were also computed over the frequencies. The most consistent observation for all these analyses is the significant activation increase at 8 Hz together with a strong correlation between the two imaging modalities.

Keywords: fMRI, EEG, Source Localization, Statistical Parametric Mapping, General Linear Model, Statistical Inference, T Test, Forward Problem, Inverse Problem, LORETA.

ÖZET

DURAĞAN HAL GÖRSEL UYARILMIŞ POTANSİYELLERDE iMRG ve EEG KAYNAK YAPILANDIRMA ARASINDAKİ İLİNTİ

Elektroensefelografi (EEG), beyin işlevlerini anlamada yaygın olarak kullanılan bir yöntemdir. Öte yandan, son yıllarda da işlevsel manyetik rezonans görüntüleme (iMRG) de bu işlev için yaygın bir araç olarak kabul görmektedir. EEG'yi diğer görüntüleme tekniklerinden ayıran en önemli özelliği yüksek zamansal çözünürlüğüdür. Ne var ki, sınırlı sayıda elektrot ölçümü ve modellemeden kaynaklanan yetersizlikler sonucu düşük nitelikli bir uzaysal çözümleme sağlamaktadır. iMRG bu süreçleri görüntülmek konusunda tatmin edici bir uzaysal çözünürlük sunarken zamansal çözünürlük açısından zayıf kalmaktadır. Bu çalışmada, EEG kaynak yapılandırma ve iMRG istatistiksel parametrik haritalama yöntemleri kullanılarak durağan hal görsel uyarılmış potansiyeller ve bunlara karşılık gelen iMRG taramaları işlenmektedir. Görsel uyarılar 2 Hz'den 10 Hz'e kadar değişmektedir. Etkinleştiği anlamlı bir şekilde belirlenmiş olan iMRG vokselleri kendilerine karşılık gelen ve aynı geometrik kafa üzerinde LORETA kullanılarak hesaplanan EEG nöroelektriksel güç ile ilintilenmiştir. Değişik frekans değerleri için uzaysal olarak ortalaması alınmış pozitif BOLD, uyarı sonrası düşüş ve LORETA genlikleri tespit edilmektedir. Bunun yanı sıra, etkinleşme maskesi üzerinde pozitif BOLD ve LORETA genlikleri arasındaki uzaysal ilintiler de hesaplanmaktadır. Son olarak, tüm uyarı frekansları için görsel uyarana dayanan bağlanım parametresi ile LORETA genlikleri arasındaki ilinti ortaya çıkarılmaktadır. Bütün bu analizlerimiz içinde en belirgin gözlem 8 Hz'deki etkinleşme şiddetindeki anlamlı artış ve yine bu frekanstaki iki farkli yöntem arasındaki yüksek ilinti olmuştur.

Anahtar Sözcükler: iMRG, EEG, Kaynak Yerelleştirimi, İstatistiksel Parametrik Eşlemleme, Genel Doğrusal Model, İstatistiksel Çıkarım, T Testi, İleri Yön Problemi, Geri Yön Problemi, LORETA.

TABLE OF CONTENTS

LIST OF FIGURES

LIST OF TABLES

LIST OF SYMBOLS

Hb	Hemoglobin
HbO_2	Oxyhemoglobin
β	Vector of parameters in the design matrix
Λ	Covariance matrix of the partial derivatives of a GRF

LIST OF ABBREVIATIONS

ERP	Event Related Potential
BOLD	Blood Oxygenated Level Dependent
fMRI	Functional Magnetic Resonance Imaging
EEG	Electroencephalography
MUSIC	Multiple Signal Classification
LORETA	Low Resolution Electro Magnetic Tomography
SPM	Statistical Parametric Mapping
GUI	Graphical User Interface
CT	Computerised Tomography
PET	Positron Emission Tomography
SPECT	Single Photon Emission Computed Tomography
MEG	Magnetoencephalography
MRI	Magnetic Resonance Imaging
EPI	Echo Planar Imaging
CBF	Cerebral Blood Flow
CBV	Cerebral Bood Volume
ISI	Inter Stimulus Interval
TR	Repetition Time
GRF	Gaussian Random Field
GLM	General Linear Model
HRF	Hemodynamic Response Function
VV	Voxel Value
EV	Explanatory Variable
SE	Standard Error
RFT	Random Field Theory
GRF	Euler Charasteristics
BEM	Boundary Element Method
ECD	Equivalent Current Dipole

SOT	Stimulus Onset Time
FEF	Frontal Eye Field
IPS	Intraparietal Sulcus
FWHM	Full Width Half Maximum
FG	Fusiform Gyrus

1. INTRODUCTION

1.1 Motivation

Localization of the cognitive activity in the brain is one of the major problems in neuroscience. Two powerful imaging modalities that are used to solve this problem are EEG and fMRI. Both methods provide valuable and reliable information about the functional activity in the brain. However, they both lack some important characteristics about the process. EEG serves very high temporal resolution when compared to other modalities like fMRI and PET. Normally, cognitive information processing consists of multiple individual stages lasting about 50-300 ms. Only EEG can reflect such instantaneous changes in detail within the range of miliseconds. However, fMRI is based on the blood flow that is caused by the neural activity. Therefore, it is limited by the indirect and temporally-delayed relation between metabolism and synaptic currents. Consequently, it's hard to visualize instantaneous activities via fMRI. On the other hand, fMRI sets the standards for spatial resolution. Since the process is performed for each individual voxel, it is much more convenient to visualize the functional activity by fMRI in this sense. Besides, a model is constructed for an fMRI analysis and for each voxel model fitting can be observed. The advantage for these techniques is that they are both non-invasive.

Development in both of the imaging modalities in the recent years raised the question "why not using both". As they have their own advantages and drawbacks, we can eliminate the weakness in both methods by using them together. In other words, one method may prove to be more efficient than the other and this will also be discussed in the results section. fMRI-constrained EEG source localization can also provide promising information in neuroscience research. Although in most cases, some discrepancy between the bioelectrical activity (EEG) and the metabolic activation (fMRI) are found, these methods usually constitute a significant common highlighted region on the cortex. Simultaneously acquired functional magnetic resonance imaging

(fMRI) and electroencephalography (EEG) data hold great promise for localizing the spatial source of neural events detected in the EEG. Despite the fact that a number of studies use this method, there has been no independent and systematic validation of the approach. Another important question is 'how similar are the results produced by these methods?'. In addition, the usage of steady state visual stimuli is important, in order to better understand the physiological changes during a stimulation. By applying a steady state stimulus we practically modulate the temporal resulotion of EEG and make it closer to that of fMRI, so that a better comparison basis is constructed.

There are a number of studies performed on the stimulus rate depending response changes. Fox et al. [1] investigated the cerebral blood flow in human striate cortex by PET where they used varying stimulus frequency. The results indicated that rCBF response had a maximum at 7.8 Hz. In another study, again rCBF response to the stimuli with different frequencies was observed and this time 7 Hz was the value that the response peaked [2]. An fMRI study, which also conforms with these results revealed that the largest MR signal was obtained at 8 Hz stimulus frequency [3]. Thomas et al. found 8 Hz as the peak response frequency in another fMRI study [4]. Ozus et al. found out that BOLD response increases up tp 6 Hz and for the higher values of frequency, it stays constant [5]. Recently, Mirzajani et al. found that BOLD response is sensitive to stimulus frequency changes and they also determined the peak response at 8 Hz [6].

1.2 Objectives

In this study, we investigate the correlation between the fMRI and source reconstructed EEG to make a comparative analysis using the steady state visual evoked responses elicited by the human brain. The steady state visual evoked potential data used for the analyses are acquired with the same paradigm. EEG raw data are processed by LORETA[7] inverse solution routines, developed in our research group, which determine the location and the moment of the dipoles. After this stage, topographic maps and localizations are depicted by various visualization tools. Different from EEG,

fMRI raw data are a series of anatomical MRI scans. During the whole fMRI analysis, SPM5 by Wellcome Department of Imaging Neuroscience was used [8]. fMRI scans, which are acquired with the same paradigm as for EEG, are subject to some spatial pre-processing. After this, the newly created pre-processed images are subject to General Linear Model (GLM) analysis followed by a statistical inference. Then, resulting statistical images are visualized using various tools. In addition, correlations between two modalities are computed on the basis of spatial activation, BOLD characteristics like positive peak and post-stimulus undershoot as well as the spatial features of these characteristics over an activation mask. In overall, we aim to introduce a novel procedural approach in quantifying the degree of spatial localization between fMRI statistical map and EEG source localization.

2. FUNCTIONAL MAGNETIC RESONANCE IMAGING (fMRI)

2.1 Neuroimaging

The idea of localization of function within the brain has only been accepted for the last century and a half. In the early 19^{th} century Gall and Spurzheim, were expelled by the scientific community for their so-called science of phrenology. They suggested that there were twenty-seven separate organs in the brain, governing various moral, sexual and intellectual traits. The importance of each to the individual was determined by feeling the bumps on their skull. The science behind this may have been wrong, but it first introduced the idea of functional localization within the brain which was developed around the mid 1800's by clinicians such as Jackson and Broca. Most of the information available on the human brain came from subjects who had sustained major head wounds, or who suffered from various mental disorders. By determining the extent of brain damage, and the nature of the loss of function, it was possible to infer which regions of the brain were responsible for which function.

Patients with severe neurological disorders were sometimes treated by removing regions of their brain. For example, an effective treatment for a severe form of epilepsy involved severing the corpus callosum, the bundle of nerve fibres which connect left and right cerebral hemispheres. Following the surgery patients were tested, using stimuli presented only to the left hemisphere or to the right hemisphere. If the object was in the right visual field, therefore stimulating the left hemisphere, then the subject was able to say what they saw. However, if the object was in the left visual field, stimulating the right hemisphere, then the subject could not say what they saw but they could select an appropriate object to associate with thant image. This suggested that only the left hemisphere was capable of speech.

With the development of the imaging techniques of computerised tomography

Table 2.1
Comparison of different neuroimaging modalities

Techniques	Resolution	Advantages	Disadvantages
SPECT	10 mm	Low cost, available	Invasive, limited resolution
PET	5 mm	Sensitive, good resolution, receptor studies	Invasive, very expensive
EEG	poor	Very low cost, high temporal resolution	Not a direct imaging technique
MEG	5 mm	High temporal resolution	Very expensive, low resolution
fMRI	3 mm	Excellent resolution, non-invasive	Limited to activation studies

(CT) and magnetic resonance imaging it was possible to be more specific as to the location of damage in brain injured patients. The measurement of the electrical signals on the scalp, arising from the synchronous firing of the neurons in response to a stimulus, known as electroencephalography (EEG), opened up new possibilities in studying brain function in normal subjects. However, it was the advent of the functional imaging modalities of positron emission tomography (PET), single photon emission computed tomography (SPECT), functional magnetic resonance imaging (fMRI), and magnetoencephalography (MEG) that led to a new era in the study of brain function.

fMRI is one of the promising neuroimaging techniques. During an fMRI experiment, the brain of the subject is scanned repeatedly, usually using the fast imaging technique of echo planar imaging (EPI). The subject is required to carry out some task consisting of periods of activity and periods of rest. During the activity, the MR signal from the region of the brain involved in the task normally increases due to the flow of oxygenated blood into that region. Signal processing is then used to reveal these regions. The main advantage of MRI over its closest counterpart, PET, is that it requires no contrast agent to be administered, and so is considerably safer. In addition, high quality anatomical images can be obtained in the same session as the functional studies, giving greater confidence as to the source of the activation. However, the function that is mapped is based on blood flow, and it is not yet possible to directly map neuroreceptors as PET can. The technique is relatively expensive, although comparable with PET, however since many hospitals now have an MRI scanner the availability

of the technique is more widespread [9].

2.2 Metabolism and Blood Flow in the Brain

The brain, like any other organ in the body requires a steady supply of oxygen in order to metabolise glucose to provide energy. This oxygen is supplied by the component of the blood called hemoglobin. It was demonstrated as long ago as 1935 that the magnetic properties of hemoglobin depended on the amount of oxygen it carried. This dependency has given rise to a method for measuring activation using MRI, commonly known as functional magnetic resonance imaging (fMRI).

The oxygen required by metabolism is supplied in the blood. Since oxygen is not very soluble in water, the blood contains a protein that oxygen can bind to, called hemoglobin. The Hemoglobin molecule is an assembly of four globular protein subunits. Chemical structure of hemoglobin is as in Fig. 2.1. Each subunit is composed of a protein chain tightly associated with a non-protein heme group. The important part of the hemoglobin molecule is an iron atom, bound in an organic structure, and it is this iron atom which gives blood it's colour. When an oxygen molecule binds to hemoglobin, it is said to be oxyhemoglobin, and when no oxygen is bound it is called deoxyhemoglobin.

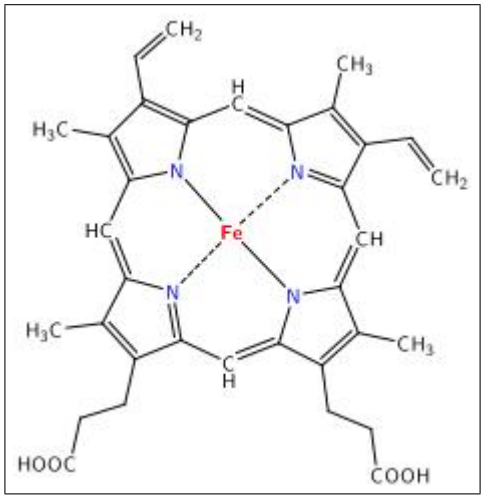

Figure 2.1 Chemical structure of a heme group in hemoglobin

To keep up with the high energy demand of the brain, oxygen delivery and blood flow to this organ is quite large. Although the brain's weight is only 2 percent of the body's, its oxygen consumption rate is 20 percent of the body's, and blood flow is 15 percent. The blood flow to the grey matter, which is a synapse rich area, is about 10 times that to the white matter per unit volume. Regulation of the regional blood flow is poorly understood, but it is known that localised neural activity results in a rapid selective increase in blood flow to that area [9].

2.3 Blood Oxygenation Level Dependent Signal Metabolism

The presence of any substance in a magnetic field alters that field to some extent. The degree of this effect is referred to as the "magnetic susceptibility". The iron in blood hemoglobin is a superb inherent magnetic susceptibility-induced T_2*-shortening intravascular contrast agent found in every tissue. It is therefore used as a local indicator of functional activation because oxygenated arterial blood contains oxygenated hemoglobin, which is diamagnetic and has a small magnetic susceptibility effect. It does not, therefore, significantly alter the regional magnetic field and does not greatly affect tissue T_2*. Deoxygenation of hemoglobin produces deoxyhemoglobin, a significantly more paramagnetic species of iron due to the four unpaired electrons, and this species disturbs the local magnetic field, B0, in a region of tissue leading to the large observed magnetic susceptibility effect. The balance of spatial and temporal alterations in local concentrations of deoxygenated to oxygenated iron affects the local observed T_2* by causing fluctuations in magnetic susceptibility. Arterially delivered blood consists mostly of oxyhemoglobin, however, as HbO2 passes through the capillary bed, the local concentration of deoxyhemoglobin (Hb) increases and often predominates. This action is illustrated in Fig. 2.2. Therefore, a T_2* gradient can exist across the vascular tree from a diamagnetic HbO_2-rich environment (with a longer relative T_2*) to a more "paramagnetic" Hb environment with a shorter T_2* [10] [11].

The local T_2* in fMRI contrast is thus determined by the balance of deoxygenated to oxygenated hemoglobin in blood within a voxel, which in turn is a function

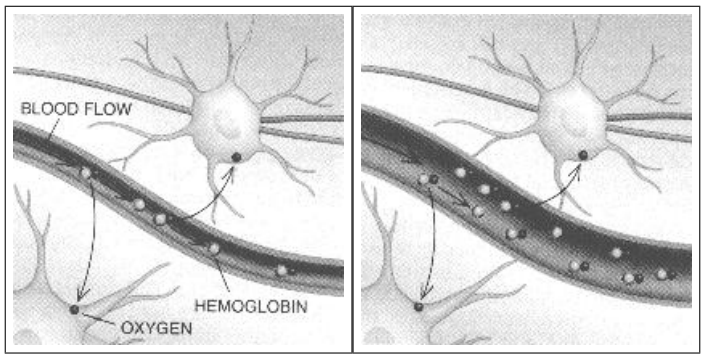

Figure 2.2 After activation, oxygen is consumed by the cells, which increases the level of deoxyhemoglobin in the blood. This is compensated for by an increase in blood flow around the active cells, leading to a net increase in oxyhemoglobin.

of local arterial autoregulation or vasodilation. By increasing the flow of oxygenated blood or reducing oxygen extraction to a region in the brain an increase in local, intravoxel T2* occurs which in turn leads to an increase in image intensity. An increase in oxygenated arterially delivered blood in response to local activation will result in more oxygenated iron in the capillary and venous vascular beds, thereby creating a relatively longer regional T_2* and an image intensity increase. It also reflects a decrease in deoxyhemoglobin content, i.e. an increase in venous blood oxygenation and a longer effective T_2*.

The image intensity for a given voxel in the brain can therefore significantly increase if more oxygenated blood enters this region and fills the venous bed. This assumes, however, that cortical activation causes local vasodilation which is not accompanied by a significant increase in oxidative metabolism. It should be remembered that local image intensity increases will also be dependent on differences in hemodynamic (blood volume, flow and oxygenation) and vessel architecture (radii, orientation, vascular openness).

As an example, visual cortex stimulation can be considered. During photic stimulation a simple presentation of flashing lights is given during an image acquisition series. The MR-observable T_2* is affected by the balance of HbO_2 to the more paramagnetic Hb existing in the capillary and venous beds. This balance produces a gradient in the local magnetic field and a potent tissue contrast mechanism because the

large surface area of the capillary bed amplifies the long range effects on the magnetic field. The photic stimulation produces rapid neuronal activation, which in turn increases cerebral blood flow (CBF), cerebral blood volume (CBV), and oxygen delivery. As CBF increases more than CBV, oxygen delivery quickly exceeds slight increases in local oxygen needs owing to the activation. Increases in local CBF in the arterioles and small arteries that occur rapidly are said to be uncoupled to local metabolism. The net effect is a surplus in the amount of oxygentated hemoglobin delivered to any activated voxel. As the delivered oxygen exceeds local demands, the capillary and venous beds fill with a larger ratio of oxygenated to deoxygenated hemoglobin compared to when the cortex was at rest. This larger amount of diamagnetic oxyhemoglobin will mean less effect from the field-altering deoxyhemoglobin, a longer T_2*, and to an increased signal on the T_2*-weighted images. The actual volume of hemoglobin in the brain is quite small (a few percent), however, the T_2* effects extends for microns beyond the vascular bed, because magnetic susceptibility is a long-range effect. This leads to approximately a 1%-10% T_2*-induced image intensity increase for a typical cortical activation task. This can be observed from intensities measured from T2*-weighted MR images or from a simple subtraction of images acquired at rest from those acquired during task [9].

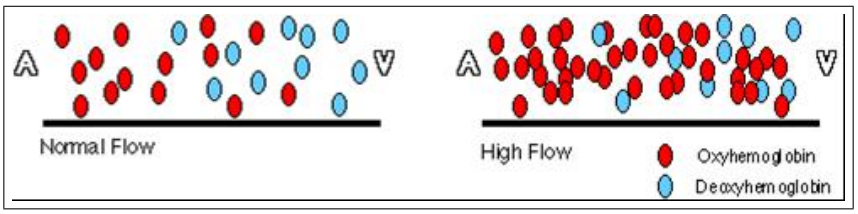

Figure 2.3 Physiological basis of a fMRI BOLD signal

2.4 Blood Oxygen Level Dependent Contrast in MR images

Since regional blood flow is closely related to neural activity, measurement of the rCBF is useful in studying brain function. It is possible to measure blood perfusion with MRI, using various techniques. However there is a sensitive contrast mechanism which depends on the blood oxygenation level, known as blood oxygen level dependent (BOLD) contrast. The mechanisms behind the BOLD contrast are still to be

determined, however there are hypotheses to explain the observed signal changes.

Deoxyhemoglobin is a paramagnetic molecule whereas oxyhemoglobin is diamagnetic. The presence of deoxyhemoglobin in a blood vessel causes a susceptibility difference between the vessel and its surrounding tissue. Such susceptibility differences cause dephasing of the MR proton signal, leading to a reduction in the value of T_2*. In a T_2* weighted imaging experiment, the presence of deoxyhemoglobin in the blood vessels causes a darkening of the image in those voxels containing vessels. Since oxyhemoglobin is diamagnetic and does not produce the same dephasing, changes in oxygenation of the blood can be observed as the signal changes in T_2* weighted images.

It would be expected that upon neural activity, since oxygen consumption is increased, the level of deoxyhemoglobin in the blood would also increase, and the MR signal would decrease. However, what is observed is an increase in signal, implying a decrease in deoxyhemoglobin. This is because upon neural activity, as well as the slight increase in oxygen extraction from the blood, there is a much larger increase in cerebral blood flow, bringing with it more oxyhemoglobin. Thus the bulk effect upon neural activity is a regional decrease in paramagnetic deoxyhemoglobin, and an increase in signal. This bulk effect is shown in Fig. 2.3.

The time course for the BOLD signal changes is delayed from the onset of the neural activity by a few seconds, and is smooth, representing the changes in blood flow that the technique detects. This is termed the 'hemodynamic response' to the stimulus. There have also been observations of an initial small 'dip' in signal before and after the larger increase in signal, possibly reflecting a transient imbalance between the metabolic activity and blood flow [9].

2.5 Functional Mapping using the BOLD Effect

To study brain function using fMRI it is necessary to repeatedly image the brain, while the subject is presented with a stimulus or required to carry out some task. The

success of the experiment is dependent on three aspects; the scanning sequence used, the design of the stimulus paradigm, and the way the data is analysed.

The magnitude of the static field used is critical to the percentage signal change obtained on activation. This is because susceptibility differences have a greater signal dephasing effect at higher fields. The earliest fMRI studies were carried out at 1.5 Tesla, but now the 3 to 4 Tesla scanners are more common. As field strength increases the magnitude of the BOLD contrast increases more rapidly than system noise, so it seems that higher field strengths are desirable, however the image quality will be reduced at higher field.

The most important aspect of the imaging sequence is that it must produce T_2* weighted images. This means that a gradient echo is most commonly used, however spin echo sequences still show BOLD contrast because of diffusion effects. Most research is carried out using EPI since its fast acquisition rate allows the activation response to short stimuli to be detected. EPI also has the benefit of reduced artefact from subject motion.

The contrast to noise ratio of the BOLD signal also depends on voxel size and slice thickness. Smaller voxels have less proton signal due to the reduced number of spins, however larger voxels may reduce the contrast to noise ratio by partial volume effects. This occurs if the signal changes on activation come from only a small region within the voxel, and so makes less of an impact on the total signal change in that voxel.

During the scanning there are a number of physiological effects that can affect results. These include cardiac pulsation, respiration and general subject movement. All these problems can be dealt with in two ways, either at the time of scanning or in image post processing. Cardiac or respiratory gating, that is triggering the scanner at one part of the cardiac cycle can be used, although this introduces artefact due to changes in the spin saturation. Postprocessing strategies have been proposed and are probably the best way to deal with this problem. Subject movement can also reduce

contrast to noise in fMRI images, and introduce artefact in the activation maps if the movement is stimulus correlated. This problem is often solved both by restraining the head of the subject and by using a postprocessing registration algorithm [9].

2.6 Paradigm Design

Designing the stimulus paradigm is as important as choosing the imaging parameters for a good experiment. A lot of experience has come from EEG and PET, but since fMRI has a temporal resolution somewhere between these two techniques new approaches can be taken.

The earliest fMRI experiments were much in the form of PET studies, that is to say a set of resting images were acquired and then a set of activation images, and one set subtracted from the other. However, since the BOLD contrast is relatively rapid in its onset and decay (of the order of a few seconds) it is possible to follow time courses for much shorter events occurring more frequently.

The most common stimulus presentation pattern is that of regular epochs of stimulus and rest, usually labelled 'on' and 'off'. The duration of these epochs needs to be long enough to accommodate the hemodynamic response, and so a value of at least 8 seconds, or more commonly 16 seconds is chosen. These epochs are repeated for as long as is necessary to gain enough contrast to noise to detect the activation response. The total experimental duration however must be a balance between how long the subject can comfortably lie still without moving, and the number of data points required to obtain enough contrast to noise. There are often some technical limitations to the experimental duration, and there is the possibility of the subject habituating to the stimulus causing the BOLD contrast to reduce with time.

Instead of epochs of stimuli, it is possible to use single events as a stimulus, much in the same way that EEG or MEG does. Again due to the hemodynamic response, these must be separated by a much longer period of time than would be required for

EEG, but since this type of stimulus presentation has the major advantage of being able to separate out the relative timings of activations in different areas of the brain. One of the major disadvantages of single event paradigms is that the experiments need to be much longer than their epoch based counterparts, in order to gain the necessary contrast to noise.

An important aspect in the design and analysis of event-related functional magnetic resonance imaging (fMRI) experiments is to optimize statistical efficiency, i.e., the accuracy with which the event-related hemodynamic response to different stimuli can be estimated for a given amount of imaging time. Several studies have suggested that using a fixed inter-stimulus-interval (ISI) of at least 15 sec results in optimal statistical efficiency or power and that using shorter ISIs results in a severe loss of power. In contrast, recent studies have demonstrated the feasibility of using ISIs as short as 500 ms while still maintaining considerable efficiency or power [12].

The choice of stimulus is very critical. For example, to activate the primary visual cortex is straightforward, but to determine the regions responsible for colour discrimination is more difficult. Ideally, it is necessary to design the 'on' and 'off' epoch such that there is only one well defined difference between them, which will only activate those brain regions responsible for the single task. This is not always possible and so a hierarchy of experiments often need to be performed. For example, to identify the regions responsible for task A, an experiment can be performed which involves task A and task B, and then one which only involves task B. The regions responsible for task A would presumably be those activated in the first experiment but not the second. This assumes that the system is a linear one, which may not be the case, or there could be some unaccounted for differences in the two paradigms, which could affect the result [9].

2.7 Analysis of fMRI Data

The analysis of fMRI data falls into two parts. Firstly the raw data must be analysed to produce an image showing the regions of activation and secondly, some level of significance must be calculated so that the probability of any of producing such a result purely by chance is suitably low.

The most straightforward way to analyse the data is to subtract the mean 'off' image from the mean 'on' image. This has the disadvantage that any small movement of the head can drastically change the pixel intensity at the boundaries of the image. This can give rise to a ring of apparent activation near the brain boundaries. To reduce this effect, and to give a statistic of known distribution, a Student's t-test can be used. This biases the result against pixels in either 'on' or 'off' set with very large variability, and so can reduce movement artefact. An image where each pixel is assigned a value based on the output of a statistical test is commonly called a statistical parametric map.

Another commonly used technique is that of correlation coefficient mapping. Here the time response of the activation to the stimulus is predicted, usually with some knowledge of the hemodynamic response, and the correlation coefficient between each pixel time course and this reference function is calculated. Other methods that have been used include Fourier transformation, which identifies pixels with a high Fourier component at the frequency of stimulus presentation, principal component analysis, which locates regions in the brain which show synchronous activity using eigenfunctions, clustering techniques, which again look for synchrony using iterative methods, and various non-parametric tests which do not require the assumption of normality in the signal distribution. All these have their various strengths and weaknesses, and no doubt new methods or variants will be developed in due course. The main criteria for any technique however is simplicity, speed, statistical validity, and sensitivity [9] [13].

Having obtained a statistical map it is necessary to display the regions of activation, together with some estimate as to the reliability of the result. If the distribution

of the statistic, under the null hypothesis of no activation present, is known, then statistical tables can be used to threshold the image, showing only those pixels which show strong stimulus correlation. When displaying the results as an image usually of several thousand pixels, it is necessary to account for multiple comparisons, since the probability of any one pixel in the image being falsely labelled as active is much greater than the probability of a lone pixel being falsely labelled. There are several ways to account for this, for example the Bonferoni correction or the theory of Gaussian random fields [14].

2.7.1 Spatial Preprocessing

The analysis of neuroimaging data generally starts with a series of spatial transformations. These transformations aim to reduce unwanted variance components in the voxel time-series that are induced by movement or shape differences among a series of scans. Voxel-based analyses assume that the data from a particular voxel all derive from the same part of the brain. Violations of this assumption will introduce artifactual changes in the voxel values that may obscure changes, or differences, of interest. The first step is to realign the data to 'undo' the effects of subject movement during the scanning session. After realignment the data are then transformed using linear or nonlinear warps into a standard anatomical space. Finally, the data are usually spatially smoothed before entering the proper analysis.

2.7.1.1 Realignment. Changes in signal intensity over time, from any one voxel, can arise from head motion and this represents a serious confound, particularly in fMRI studies. Despite restraints on head movement, co-operative subjects still show displacements of up several millimeters. Realignment involves (i) estimating the 6 parameters of an affine 'rigid-body' transformation that minimizes the sum of squared differences between each successive scan and a reference scan (usually the first or the average of all scans in the time series) and (ii) applying the transformation by re-sampling the data using tri-linear, sinc or spline interpolation. Estimation of the

affine transformation is usually effected with a first order approximation of the Taylor expansion of the effect of movement on signal intensity using the spatial derivatives of the images. However, in fMRI, even after perfect realignment, movement-related signals can still persist. This calls for a further step in which the data are adjusted for residual movement-related effects [14].

Temporal realignment also needs to be performed in preprocessing steps. A high temporal resolution is always desired. Recent developments in rapid echo-planar functional resonance imaging (fMRI) and event-related analyses combine a spatial resolution of millimetres with a temporal resolution of seconds. A fundamental trade-off remains however: large brain coverage at high spatial resolution requires many, thin image planes (slices), resulting in a longer interscan interval (TR) and poorer temporal resolution. Although regular stimulus times with respect to scan times allow a higher effective sampling rate, existing volume-based analysis techniques such as SPM assume simultaneous sampling of all slices. Interpolation of data in time is a solution to solve the slice timing problem [15] [16].

2.7.1.2 Adjusting for Movement Related Effects in fMRI. In extreme cases as much as 90% of the variance, in fMRI time-series, can be accounted for by the effects of movement after realignment. Causes of these movement-related components are due to movement effects that cannot be modeled using a linear affine model. These non-linear effects include; (i) subject movement between slice acquisition, (ii) interpolation artifacts, (iii) nonlinear distortion due to magnetic field inhomogeneities and (iv) spin-excitation history effect. The estimated movement-related signal is simply subtracted from the original data. This adjustment can be carried out as a pre-processing step or embodied in model estimation during the proper analysis [14].

2.7.1.3 Spatial Normalization. After realigning the data, a mean image of the series, or some other co-registered (e.g. a T1-weighted) image, is used to estimate some warping parameters that map it onto a template that already conforms to some

standard anatomical space (e.g. Talairach and Tournoux 1988). This estimation can use a variety of models for the mapping, including: (i) a 12-parameter affine transformation, where the parameters constitute a spatial transformation matrix, (ii) low frequency basis spatial functions (usually a discrete cosine set or polynomials), where the parameters are the coefficients of the basis functions employed and (iii) a vector field specifying the mapping for each control point (e.g. voxel). In the latter case, the parameters are vast in number and constitute a vector field that is bigger than the image itself. Estimation of the parameters of all these models can be accommodated in a simple Bayesian framework, in which one is trying to find the deformation parameters that have the maximum posterior probability given the data y, where. Put simply, one wants to find the deformation that is most likely given the data. This deformation can be found by maximizing the probability of getting the data, assuming the current estimate of the deformation is true, times the probability of that estimate being true. In practice, the deformation is updated iteratively using a Gauss-Newton scheme to maximize. The likelihood potential is generally taken to be the sum of squared differences between the template and deformed image and reflects the probability of actually getting that image if the transformation was correct [14] [17].

2.7.1.4 Co-registration of functional and anatomical data. It is sometimes useful to co-register functional and anatomical images. However, with echo-planar imaging, geometric distortions of T_2* images, relative to anatomical T1-weighted data, are a particularly serious problem because of the very low frequency per point in the phase encoding direction. Typically for echo-planar fMRI magnetic field inhomogeneity, which is sufficient to cause dephasing of 2π through the slice, corresponds to an in-plane distortion of a voxel. 'Unwarping' schemes have been proposed to correct for the distortion effects (Jezzard and Balaban 1995). However, this distortion is not an issue if one spatially normalizes the functional data [14].

2.7.1.5 Spatial smoothing. The motivations for smoothing the data are as follows: (i) By the matched filter theorem, the optimum smoothing kernel corresponds to

the size of the effect that one anticipates. The spatial scale of hemodynamic responses is, according to high-resolution optical imaging experiments, about 2 to 5mm. Despite the potentially high resolution afforded by fMRI an equivalent smoothing is suggested for most applications. (ii) By the central limit theorem, smoothing the data will render the errors more normal in their distribution and ensure the validity of inferences based on parametric tests. (iii) When making inferences about regional effects using Gaussian random field theory the assumption is that the error terms are a reasonable lattice representation of an underlying and smooth Gaussian field. This necessitates smoothness to be substantially greater than voxel size. If the voxels are large, then they can be reduced by sub-sampling the data and smoothing (with the original point spread function) with little loss of intrinsic resolution. (iv) In the context of inter-subject averaging it is often necessary to smooth more (e.g. 8 mm in fMRI or 16mm in PET) to project the data onto a spatial scale where homologies in functional anatomy are expressed among subjects [14].

2.7.2 Statistical Parametric Mapping and Statistical Analysis

Functional mapping studies are usually analyzed with some form of statistical parametric mapping. Statistical parametric mapping requires some statistical processes to test hypotheses about regionally specific effects. Statistical parametric mapping usually refer to the conjoint use of the general linear model (GLM) and Gaussian random field (GRF) theory to analyze and make classical inferences about spatially extended data through statistical parametric maps (SPMs). The GLM is used to estimate some parameters that could explain the input raw data for each voxel. GRF theory is used to resolve the multiple comparison problem when making inferences over a volume of the brain. GRF theory provides a method for correcting p values for the search volume of a SPM and plays the same role for continuous data as the Bonferoni correction for the number of discontinuous or discrete statistical tests [14]. An overview of Statistical Parametric Mapping is visualized as in Fig. 2.4.

Statistical parametric mapping (SPM) is a mass univariate approach to modeling

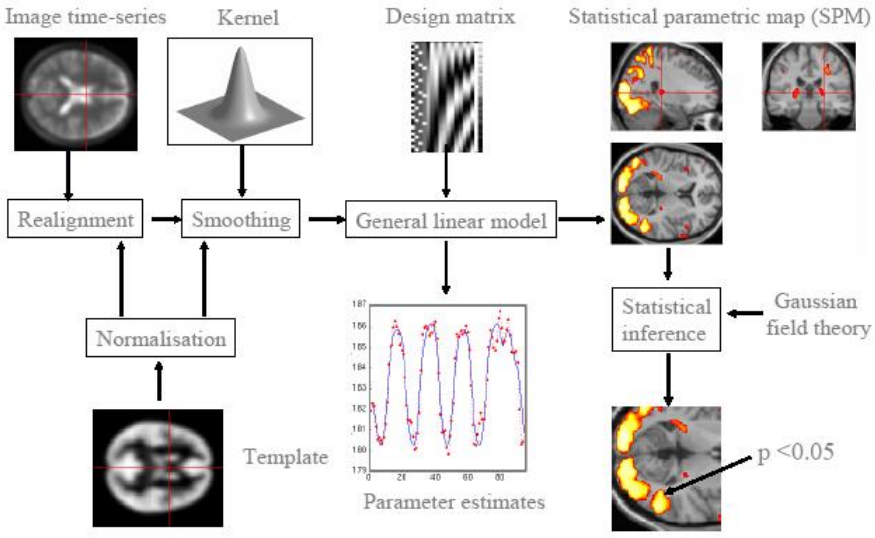

Figure 2.4 An overview of Statistical Parametric Mapping. Courtesy of Wellcome Department of Imaging Neuroscience.

spatiotemporal neuroimaging data. SPM was originally developed to propose solutions to metabolic or hemodynamic imaging time series such as PET, SPECT, and fMRI data. However, similar spatiotemporal models have also been derived for EEG data. Several studies have been performed to illustrate the efficiency of SPM techniques through applications of SPM to EEG data. For example, Bosch-Bayard et al. [18] have described an SPM approach to source reconstructed Fourier transformed EEG data. Park et al. [19] have implemented a procedure that produces statistical parametric maps with source reconstructed EEG data. Barnes and Hillebrand [20] have applied SPM to source reconstructed MEG data. These studies prove SPM as a powerful tool for different types of modalities [21].

2.7.2.1 General Linear Model. Statistical analysis of imaging data involves modeling the data to partition observed responses into components of interest, confounds and error and making inferences about the interesting effects in relation to the error variance. This classical inference can be regarded as a direct comparison of the variance due to an interesting experimental manipulation with the error variance. Alternatively, one can view the statistic as an estimate of the response, or difference of

interest, divided by an estimate of its standard deviation. This is a useful way to think about the T statistic.

The general linear model is an equation that expresses the observed response variable Y in terms of a linear combination of explanatory variables X plus a well behaved error term. The general linear model is variously known as 'analysis of covariance' or 'multiple regression analysis'. The matrix X that contains the explanatory variables (e.g. designed effects or confounds) is called the design matrix. Each column of the design matrix corresponds to some effect one has built into the experiment or that may confound the results. These are referred to as explanatory variables, covariates or regressors.

The equations related to GLM can be used to implement a range of statistical analyses. The issue is therefore not so much the mathematics but the formulation of a design matrix X appropriate to the study design and inferences. The design matrix can contain both covariates and indicator variables. Each column of X has an associated unknown parameter. Some of these parameters will be of interest (e.g. the effect of particular sensorimotor or cognitive condition or the regression coefficient of hemodynamic responses on reaction time). The remaining parameters will be of no interest and belongs to confounding effects (e.g. the effect of being a particular subject or the regression slope of voxel activity on global activity). Inferences about the parameter estimates are made using their estimated variance. This allows one to test the null hypothesis that all the estimates are zero using the F statistic or that some particular linear combination (e.g. a subtraction) of the estimates is zero using T statistic. The T statistic obtains by dividing a contrast or compound (specified by contrast weights) of the ensuing parameter estimates by the standard error of that compound. The latter is estimated using the variance of the residuals about the least-squares fit. An example of a contrast weight vector would be [-1 1 0 0.....] to compare the difference in responses evoked by two conditions, modeled by the first two condition-specific regressors in the design matrix [22][14].

The aim of the general linear model is to explain the variation of the time course

y1...yi...yn, in terms of a linear combination of explanatory variables and an error term. For a simple model with only one explanatory variable x1...xi...xn, the general linear model can be written as

$$y_i = x_i\beta + \epsilon_i \tag{2.1}$$

where β is the scaling, or slope parameter, and e_i is the error term. If the model includes more variables it is convenient to write the general linear model in matrix form as

$$\mathbf{Y} = \mathbf{X}\beta + \epsilon \tag{2.2}$$

where Y is the vector of observed pixel values, β is the vector of parameters and e is the vector of error terms. The matrix X is known as design matrix. Its number of rows is equal to the number of scans in the experiment and its column number is equal to the number of explanatory variables. β can be determined by solving the 'normal equations':

$$X^TY = (X^TX)\beta' \tag{2.3}$$

where β' is the best linear estimate of beta. Provided that (X^TX) is invertable then β' is given by

$$\beta' = (X^TX)^{-1}X^TY \tag{2.4}$$

Such parameter estimates are normally distributed, and since the error term can be determined, statistical inference can be made as to whether the β parameter corresponding to the model of an activation response is significantly different from the null hypothesis. The general linear model provides a framework for modeling of the data, and can eliminate effects that may deteriorate the analysis, such as drift or respiration, provided that they can be modeled and placed properly in the design matrix [23][14].

2.7.2.2 Hemodynamic Impulse Response and Temporal Basis Functions.

An early observation regarding blood oxygen level dependent (BOLD), functional mag-

netic resonance imaging (fMRI) data is that a sudden change in neural activity produces a signal change that takes several seconds to develop and decay [24]. The slow nature of the BOLD fMRI signal is a consequence of its hemodynamic origins. Changes in neural activity cause changes in the local vasculature and the local deoxyhemoglobin concentration, to which BOLD is sensitive. Therefore, BOLD fMRI provides a measure of the local, temporal pattern of neural activity, but only after that pattern has passed through a hemodynamic filter that smoothes and delays the signal. Since the majority of BOLD fMRI experiments test hypotheses regarding neural activity, as opposed to vascular physiology, methods have been developed to account for the temporal blurring imposed by the natural hemodynamic filter.

The particular time-course of fMRI signal change that follows a brief period of neural activity can be termed the hemodynamic response. Previously, it was proposed that an estimated hemodynamic response (treated as the impulse response function of a linear system) can be used to obtain a predicted fMRI signal response for any arbitrary pattern of neural activity [25]. These predicted signal responses can be used to test hypotheses regarding the effect of experimental treatments upon neural activity. Since this approach more accurately predicts the shape of the fMRI signal, it provides greater statistical sensitivity and validity [26].

To make statistical inferences about activations in fMRI with the GLM, we need some core functions to explain the local activity. An impulse response function is the response to a single impulse, measured at a series of times after the input. It characterizes the input-output behavior of the system (i.e. voxel) and places important constraints on the sorts of inputs that will excite a response. The hemodynamic response functions (HRFs) were estimated [25] and those HRFs resembled a Poisson or Gamma function, peaking at about 5 seconds. Our understanding of the biophysical and physiological mechanisms that lie under the HRF has grown considerably in the past few years [27]. A typical hemodynamic impulse response function looks like something in Fig. 2.5.

Knowing the forms that the HRF can take is important, because it allows for

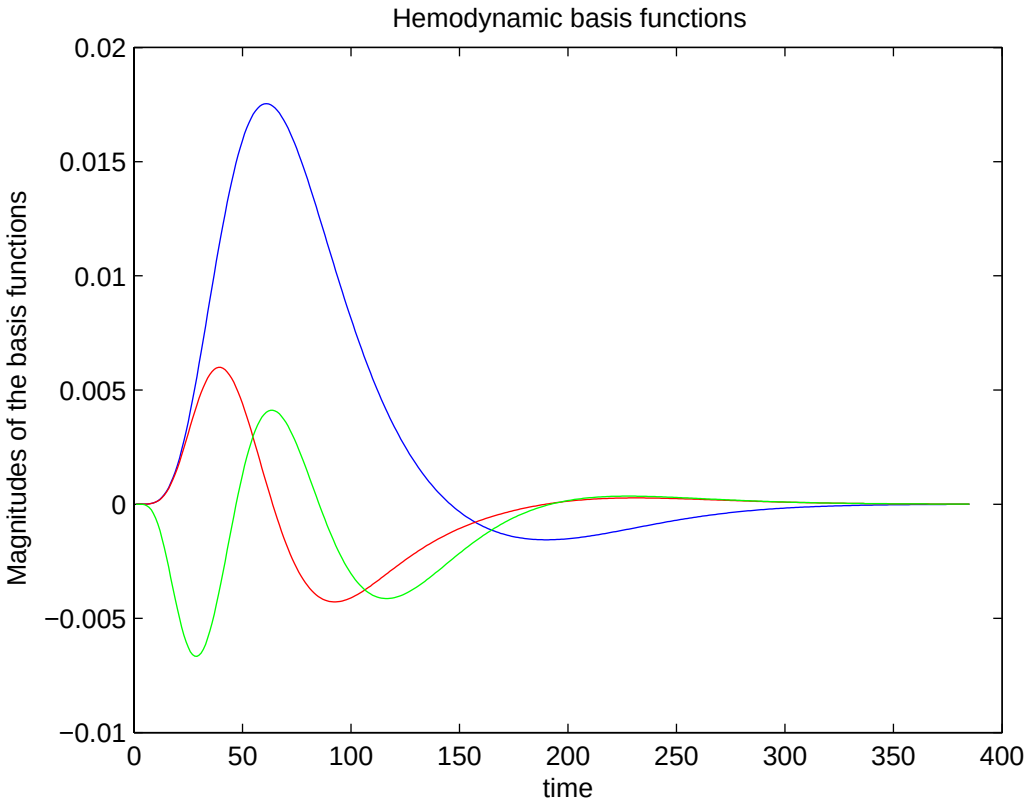

Figure 2.5 Hemodynamic Basis Functions

better statistical models of the data. Besides, HRF may vary from voxel to voxel and this has to be accommodated in the GLM. To allow for different HRFs in different brain regions the notion of temporal basis functions, to model evoked responses in fMRI, was introduced [23] and later applied to event-related responses [28]. The basic idea behind temporal basis functions is that the hemodynamic response induced by any given trial type can be expressed as the linear combination of several basis functions of peristimulus time. The convolution model for fMRI responses takes a stimulus function encoding the supposed neuronal responses and convolves it with an HRF to give a regressor that enters into the design matrix. When using basis functions, the stimulus function is convolved with all the basis functions to give a series of regressors. The associated parameter estimates are the coefficients or weights that determine the mixture of basis functions that best models the HRF for the trial type and voxel of concern. We find the most useful basis set to be a canonical HRF and its derivatives with respect to the key parameters that determine its form (e.g. latency and dispersion). The nice thing about this approach is that it can partition differences among evoked responses into

differences in magnitude, latency or dispersion, that can be tested for using specific contrasts [29].

2.7.2.3 Hypothesis Testing. After the parameter estimates and related residual errors are calculated, the null hypothesis needs to be tested. Null hypothesis is equivalent to saying that 'there is no relationship between the initial voxel value (VV) and the explanatory variable (EV)'. There are several ways to test it, but t test is simple and convenient. The reason for determining the slopes (beta coefficients) of the EVs is because we think that VVs increase linearly with increasing EV. We can assess whether this is the case, because, if so, there will be a positive slope linking EV with the VVs. We test this against the null hypothesis. The null hypothesis is that there is no relationship between EV and the voxel data. On the null hypothesis, β, the slope of the line, will not be significantly different from zero. We can test this by making a t statistic, where the t statistic is [14]:

$$\beta/SE \tag{2.5}$$

and where SE is the standard error of the slope.

This t statistic will be large and positive if the slope is significantly greater than 0, and large and negative if the slope is significantly less than 0. When the design matrix has many columns, it is useful to express our hypothesis with a more general mechanism, called a "contrast". This mechanism is used to express hypotheses about the effects defined in the design matrix. In fact, the question roughly becomes; given the error in our observations, could this estimate that we have of the slope (beta) has arisen by chance, even if the null hypothesis is true? On the other hand, is beta too large for this to be satisfactory? So, the t statistic is our least squares estimate of the slope, divided by a measure of the error of the slope, and is therefore an index of how far the slope differs from zero, given the error. We already know the distribution of

the t statistic. Therefore, for instance, we can say that, by chance, with 10 degrees of freedom, a t statistic of 8.5 or greater occurs 0.01 percent of the time, if the null hypothesis is true (the p value is 0.0001). After completing the null hypothesis testing, what we have is a brain image of t values, which indicates the regions on the cortex with highest probability that the activation occurred. One slice of a t-statistic image is illustrated in Fig. 2.6.

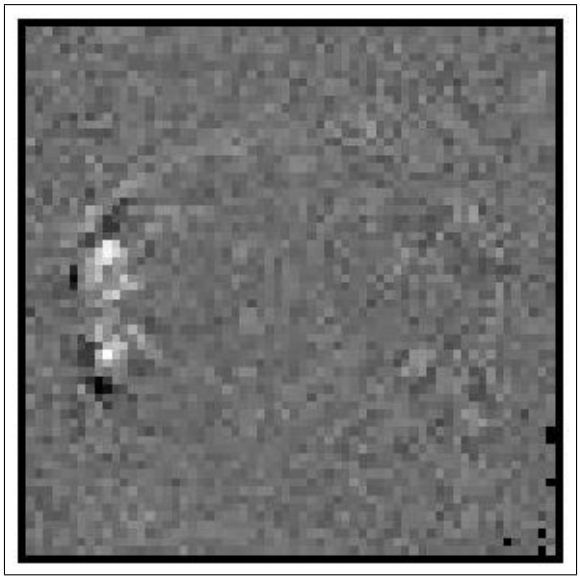

Figure 2.6 One slice of a statistical t image obtained from a fMRI retinotopy study

2.7.2.4 Statistical Inference and Random Field Theory. With an anatomically open hypothesis (i.e. a null hypothesis that there is no effect anywhere in a specified volume of the brain) a correction for multiple dependent comparisons is necessary. The theory of random fields provides a way of adjusting the p-value that takes into account the fact that neighboring voxels are not independent by virtue of continuity in the original data. Provided the data are sufficiently smooth the GRF correction is more sensitive than a Bonferroni correction for the number of voxels. GRF theory deals with the multiple comparisons problem in the context of continuous, spatially extended statistical fields, in a way that is analogous to the Bonferroni procedure for families of discrete statistical tests. When declaring a connected volume or region of statistical parametric map (SPM) to be significant, we refer collectively to all the voxels that comprise that volume. The false positive rate is expressed in terms of connected

sets of voxels above some threshold, under the null hypothesis of no activation. This is not the expected number of false positive voxels. One false positive region may contain hundreds of voxels, if the SPM is very smooth. A Bonferroni correction would control the expected number of false positive voxels, whereas GRF theory controls the expected number of false positive regions. Because a false positive region can contain many voxels the corrected threshold under a GRF correction is much lower, rendering it much more sensitive. In fact the number of voxels in a region is somewhat irrelevant because it is a function of smoothness. The GRF correction discounts voxel size by expressing the search volume in terms of smoothness or resolution elements (resels) [30] [31].

Normally, some degree of spatial correlation exists in functional imaging data. In general, data from any one voxel in the functional image tend to be similar to data from nearby voxels. Therefore, the errors from the statistical model will tend to be correlated for nearby voxels. Typically, we realign images for a subject to correct for motion during the scanning session, and we usually spatially normalize a subject's brain to a template to compare data between subjects. These transformations require the creation of new resampled images, which have voxel centres that are very unlikely to be the same as those in the original images. The resampling requires that we estimate the signal for these new voxel locations from the values in the original image, and typical resampling methods require some degree of averaging of neighbouring voxels to produce new voxel value.

Smoothing is a very common method in preprocessing the functional images before statistical analysis. A proportion of the noise in functional images is independent from voxel to voxel, whereas the signal of interest usually extends over several voxels. This is because of the possibly distributed nature of neuronal sources and the spatially extended nature of the hemodynamic response. According to the matched filter theorem smoothing improves the signal to noise ratio. Besides, smoothing involves averaging over voxels, which will by definition increase spatial correlation [32]. An example of a smoothed image is seen below in Fig. 2.7.

When we smooth an image with a smoothing kernel such as a Gaussian, each value in the image is replaced with a weighted average of itself and its neighbours. 2.7 shows a smoothed image with a Gaussian kernel of Full Width at Half Maximum (FWHM) of 10 pixels. An FWHM of 10 pixels means that, at five pixels from the centre, the value of the kernel is half its peak value. Smoothing has the effect of blurring the image, and reduces the number of independent observations.The smoothed image contains spatial correlation, which is typical of the output from the analysis of functional imaging data. However, since there is no simple way of calculating the number of independent observations in the smoothed data, we need to use random field theory for this [32]. In RFT implementation, we first estimate the smoothness (spatial correlation) of our statistical map. Then we use the smoothness values in the RFT equation, to give the expected Euler Characteristic at different thresholds.

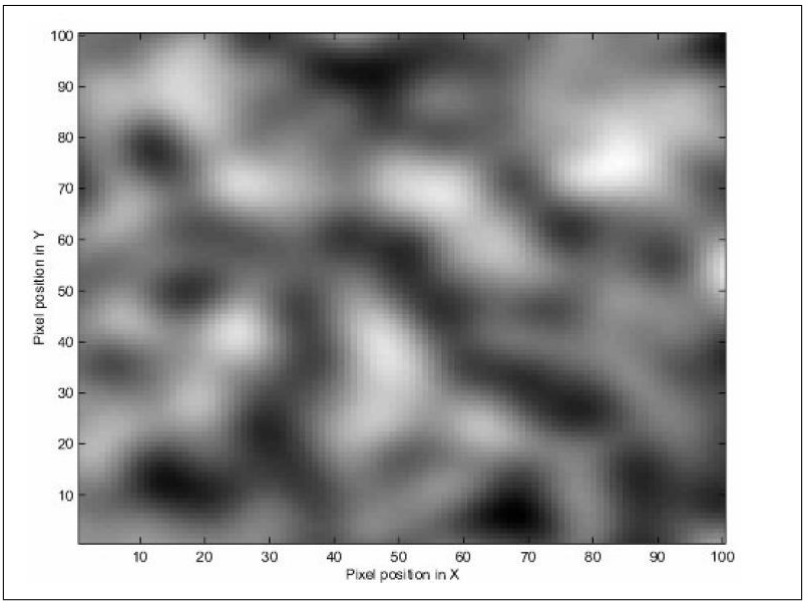

Figure 2.7 A smoothed 100x100 image with a Kernel of FWHM of 10 pixels

The smoothness of a stationary GRF is defined as $|\Lambda|^{-1/2}$, where Λ is the covariance matrix of the partial derivatives of the GRF at any voxel position. Usually we do not know the smoothness of our statistical map. Even if the image is smoothed this is true, because we usually do not know the extent of spatial correlation in the underlying data before smoothing. If we do not know the smoothness, it can be calculated using the observed spatial correlation in the images [33] [34].

To test for the significance for an activation intensity in a SPM, it is necessary to evaluate the probability that the maximum value in the map is greater than a given threshold t under null hypothesis. To apprpximate this probability, Euler characteristic (EC) of a binarised map thresholded at t was proposed [35]. Euler characteristic is a geometrical measure that counts the number of connected components minus the number of holes in the image volume. However, in the high thresholds, EC corresponds to the number of regions above the threshold value [36] [37]. The expected Euler Characteristic is defined as follows:

$$E[x_t] = \lambda(V)\,|\Lambda|^{1/2}\,(2\pi)^{-(D+1)/2} H_{e_{D(t)}} e^{-t^2/2} \tag{2.6}$$

where $\lambda(V)$ is the volume that is analyzed. $H_{e_{D(t)}}$ is the Hernite polynomial of degree D in t. Here threshold t is not specified by the user. The value of t is simply the local maxima or any value that is tested, as opposed to the threshold used for spatial extent tests. $|\Lambda|$ is the covariance matrix of the partial derivative of the process in the D directions of space and it is crucial for the assessment of $E[x_t]$ and the calculation of the p values.

3. IMPLEMENTATION and RESULTS

3.1 Experiment Paradigm and Data Specifications

The dataset was obtained from the experiments that were performed in the EEG lab of the Physiology department and the MRI room of the radiology department at the medical faculty of Istanbul University. This dataset includes both EEG and fMRI data obtained with the same paradigm. The experiments were performed on a single subject. In these sessions, single shot T2* weighted gradient EPI sequence was used. 89 functional EPI images with 20 slices were acquired for each temporal frequency value of the stimuli. Various frequencies were used during the experiment. These values range from 1 Hz to 100 Hz. Repetition time for the stimuli is 2 seconds and the photic stimulation was applied by a LED on goggles. EEG data was recorded from 30 channel with BrainAmp MR+ amplifier.

3.2 Evaluation and Results for fMRI

The results are analyzed using SPM5 software of Wellcome Department of Imaging Neuroscience [8]. Firstly, the fMRI scans are directed to a preprocessing before GLM analysis. Spatial and temporal alignments are performed in order to undo the effects that appeared during data acquisition. These steps are followed by a coregistration of functional and anatomical images. Here we use a 2 mm template to register the mean image and all functional scans together with this template image. Spatial normalization is performed in order to fit the subject's brain image into our standard template, which we use also to depict the EEG inverse solution results. In this way, we can construct a comparison base for the results from both modalities. As the last step of spatial preprocessing, for the enhancement of the signal to noise ratio, spatial smoothing with a 8 mm Kernel is performed. After this step, images are ready to undergo a GLM analysis, where the regressors are categorized according to a single

variable, which is the 'visual effect'. In addition, a column for a baseline is also added. Design matrix was formed and parameters were estimated according to this matrix. Finally, statistical inference is performed using appropriate values for height and spatial extent. This procedure was repeated for the stimulus frequency values 2,4,7,8 and 10 Hz. The Fig. 3.1 below shows the activation responses for the stimulus frequencies of 2,4,7,8 and 10 Hz.

3.3 Evaluation and Results for EEG

EEG has been recorded from 30 channel with BrainAmp MR+ amplifier in the EEG lab of the Physiology department of Istanbul University Medical Faculty. The signals are analog filtered between 0.1-250 Hz and digitized at 1000 samples/sec. The data channels used are Oz, O1, O2, Pz, P3, P4, P7, P8, Cz, C3, C4, T7, T8, Fz, F3, F4, FCz, FC3, FC4, CPz, CP3, CP4, FT7, FT8, F7, F8, TP7, TP8, FP1, FP2. EEG source reconstruction is performed using LORETA inverse solution developed by our group. The basic motivation for using the LORETA algorithm as an inverse problem solver is to obtain a distributed electric source configuration throughout the brain volume. This enables us to make a correlative comparison between the EEG and fMRI source distributions over a well defined activation mask. The head model used in this study is developed using the average T1 weighted human brain MRI data provided by Montreal Neurology Institute (MNI). SPM5 [8] is used for 3D segmentation of the brain, skull and scalp. After segmentation, the surfaces are triangulated in order to generate the realistic head model that we need to solve the forward problem. The routine is applied to the instantaneous multichannel data of the fundamental frequency for each stimulus frequency. Figure 3.2 shows the multi-channel raw EEG data for different frequencies. Figures 3.3-3.7 depict the LORETA inverse solution results for the frequencies varying from 2 to 10 Hz. Besides, potential distributions can be seen in Fig. 3.8.

3.4 fMRI and EEG Responses at Different Frequencies

Results derived also in terms of the BOLD-fMRI and EEG signal responses are shown in Fig. 3.10 and 3.11. For each stimulus frequency, raw fMRI scans are analyzed and the voxel values within the region of interest, i.e., V1 for this experiment, are averaged. Spatially averaged BOLD response for one stimulus temporal frequency can be seen in Fig. 3.9. For this process, at the same time instance, BOLD signals at each supra-threshold voxels are averaged and this is repeated for the whole time series. Also for each frequency, maximum response from a single supra-threshold voxel is recorded and the average of all these voxels is computed. By doing this, we can show the spatially averaged BOLD response with respect to frequency values as seen in Fig. 3.10(a). Similarly, we also performed the same thing for the minimum BOLD response and the spatially averaged post-stimulus undershoot behavior can be observed in Fig. 3.10(b). From the same region, LORETA potentials are evaluated and their absolute values are averaged for EEG response which is visualized in Fig. 3.10(c). Spatial correlation of the positive maximum BOLD response and the EEG is also studied. Peak of the BOLD response is computed for the supra-threshold voxels and the correlation coefficients for this set of data and the corresponding EEG LORETA magnitudes. These correlation coefficients can be seen for different frequencies in Fig. 3.11.

3.5 Correlation Between fMRI and EEG at Different Frequencies

Another important assessed criterion is the spatial correlation between fMRI activation and EEG inverse solution results. This is performed to determine how similar the activation points are in the two modalities. First of all, this process requires that the results are expressed on a common spatial template. To achieve this, the functional MR images are coregistered and normalized to a standard 2 mm template image. Also for the source reconstruction in EEG, the same template is used. In this way, we can

observe the correlation between the two modalities. Among the 43277 data points on the statistical t image that was constructed after fMRI analysis, around $300-350$ points are chosen by appplying a height threshold. The regions that are corresponding to the same location on the brain are determined by using the MNI coordinate system. Then the values coming from both modalities are assessed based on correlation for different frequency values. The resulting correlation coefficients can be observed in Fig. 3.12 for different values of stimulus temporal frequency.

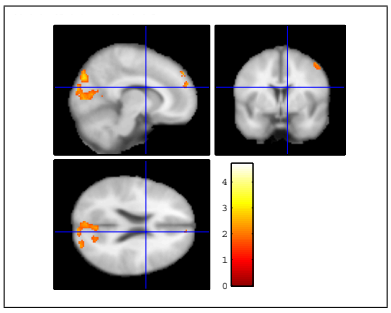

(a) Activation map for 2 Hz at p=0.05 and ext=50

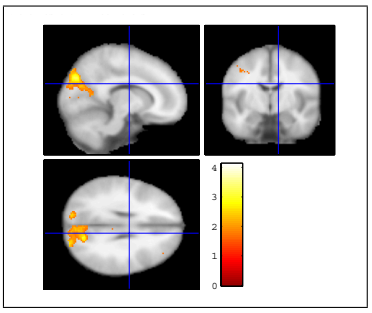

(b) Activation map for 4 Hz at p=0.05 and ext=50

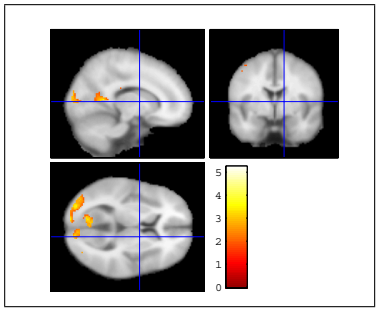

(c) Activation map for 7 Hz at p=0.03 and ext=50

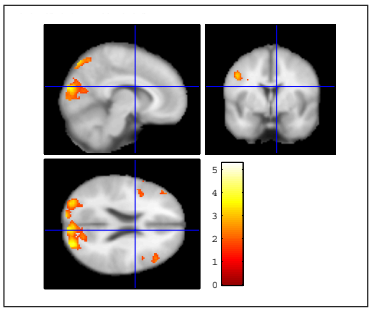

(d) Activation map for 8 Hz at p=0.05 and ext=50

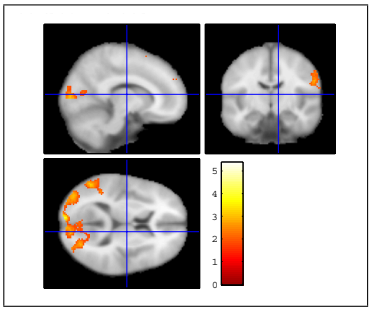

(e) Activation map for 10 Hz at p=0.04 and ext=75

Figure 3.1 fMRI activation maps for different frequencies

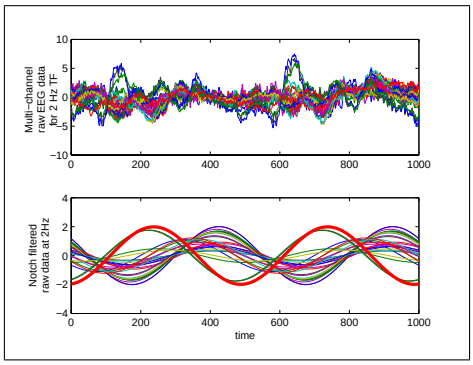

(a) EEG raw data for 2Hz temporal frequency

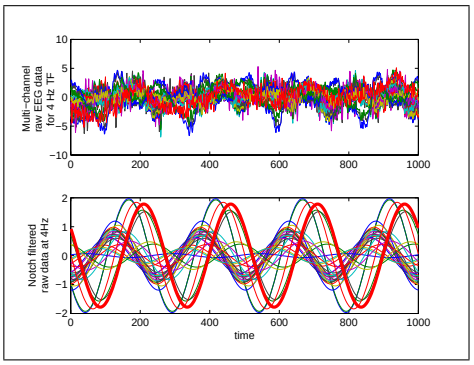

(b) EEG raw data for 4Hz temporal frequency

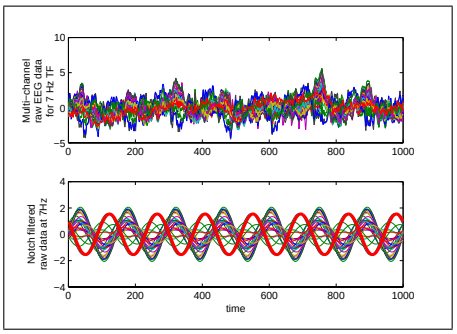

(c) EEG raw data for 7Hz temporal frequency

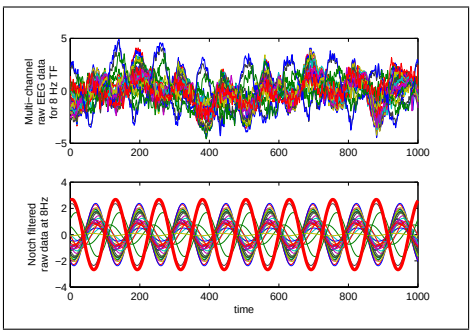

(d) EEG raw data for 8Hz temporal frequency

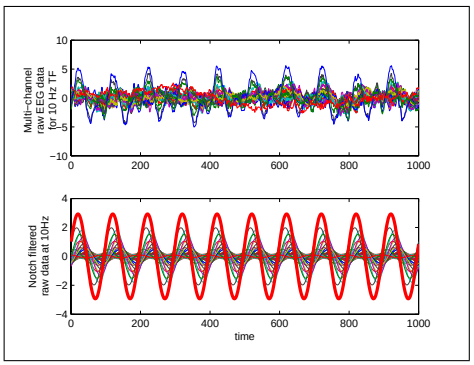

(e) EEG raw data for 10Hz temporal frequency

Figure 3.2 Multi-channel raw EEG data for different frequencies

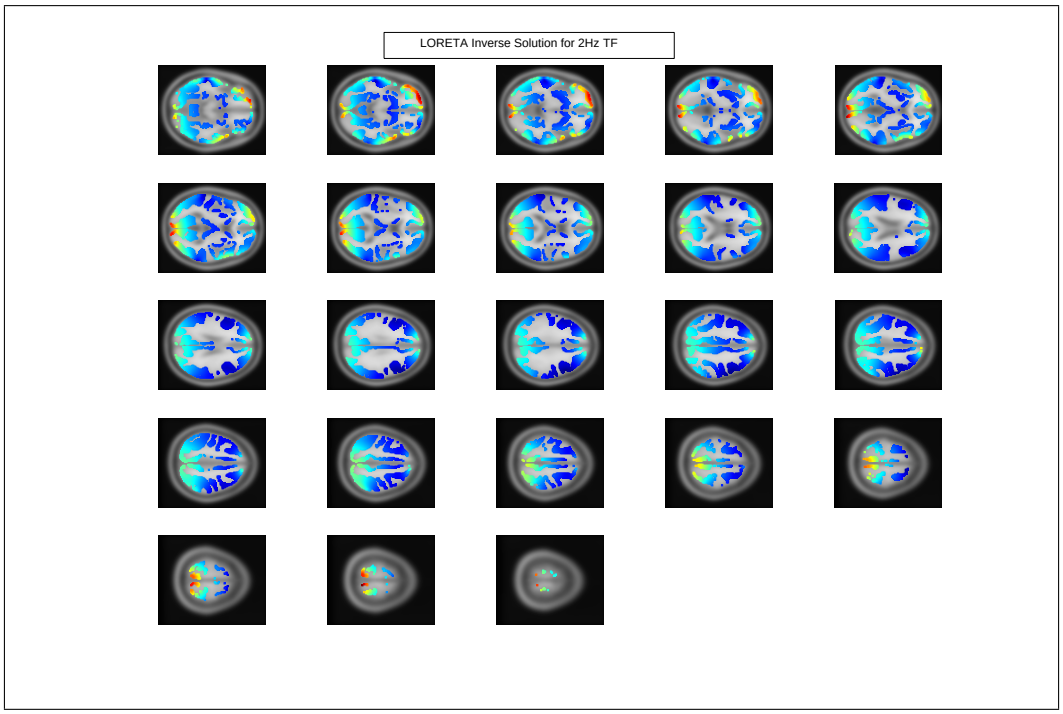

Figure 3.3 LORETA inverse solution for 2 Hz temporal frequency

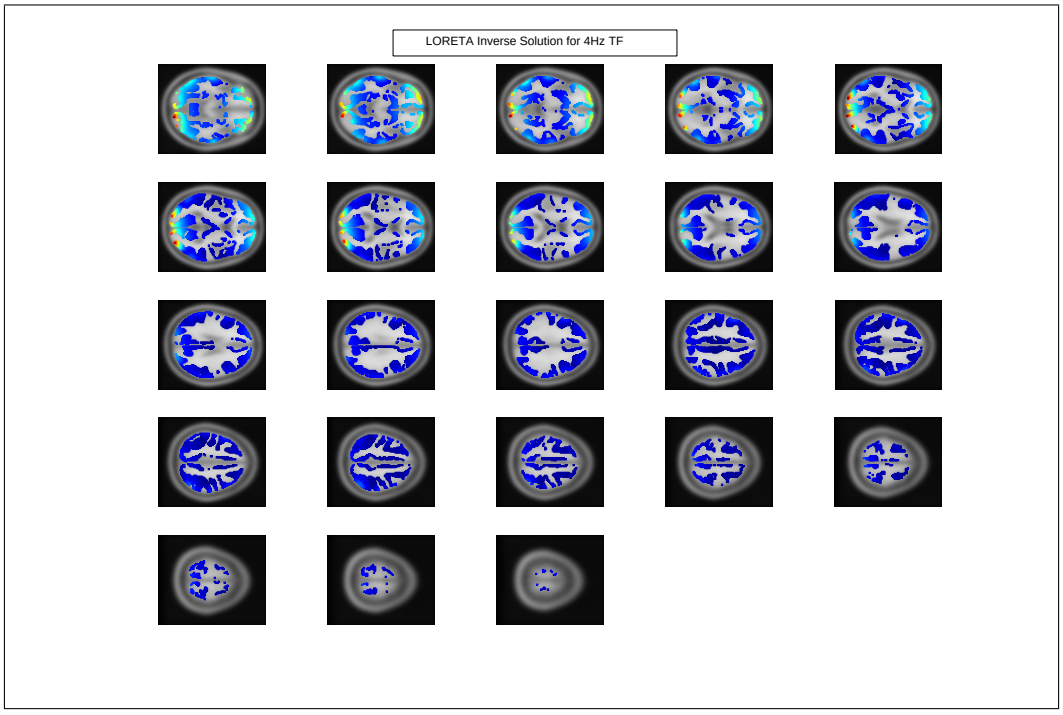

Figure 3.4 LORETA inverse solution for 4 Hz temporal frequency

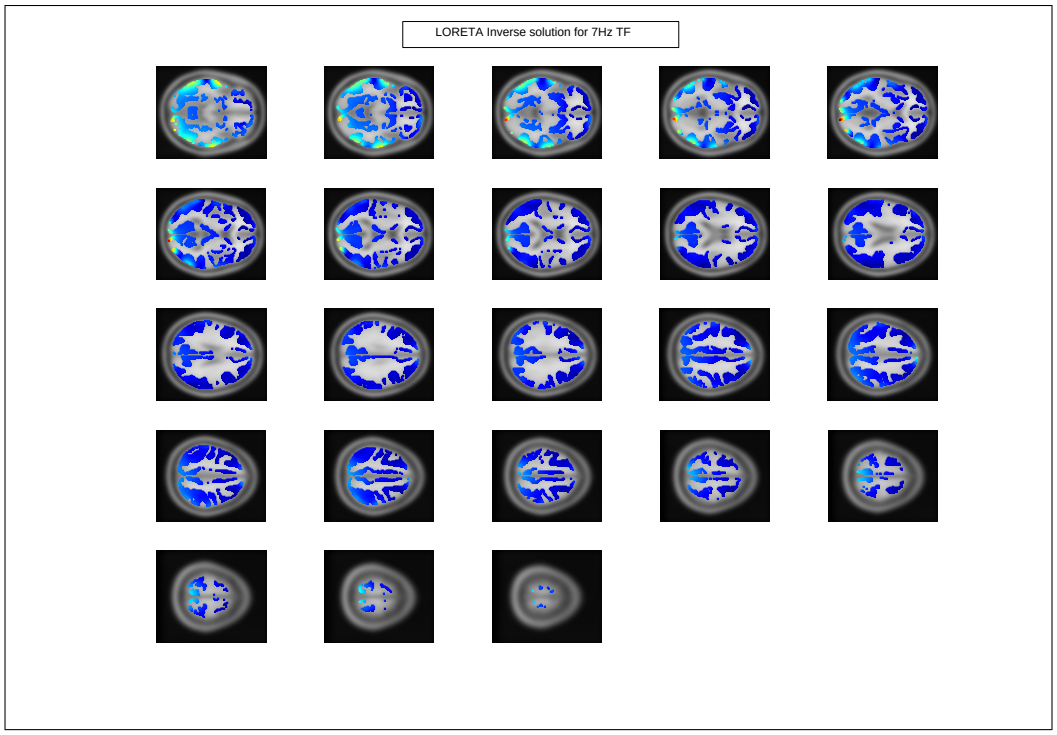

Figure 3.5 LORETA inverse solution for 7 Hz temporal frequency

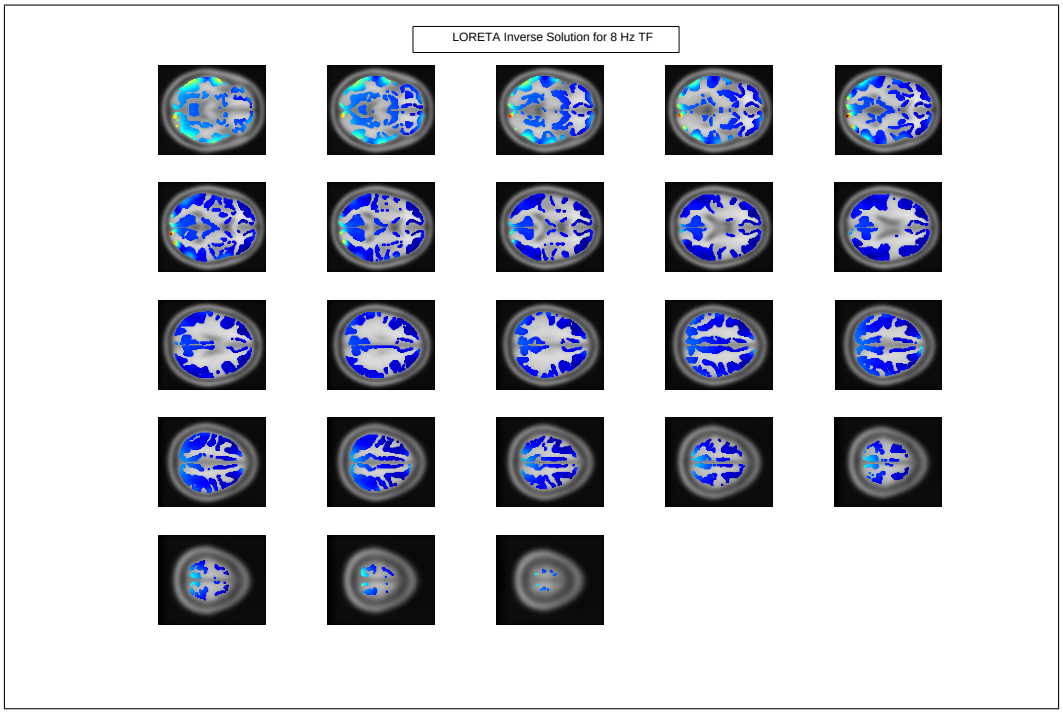

Figure 3.6 LORETA inverse solution for 8 Hz temporal frequency

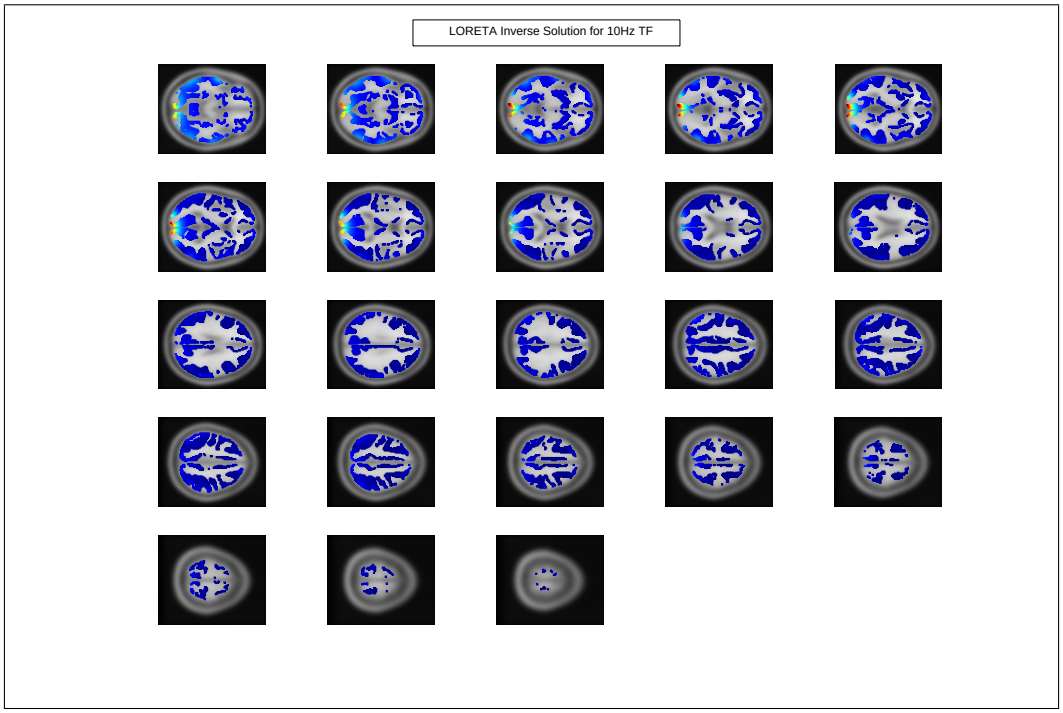

Figure 3.7 LORETA inverse solution for 10 Hz temporal frequency

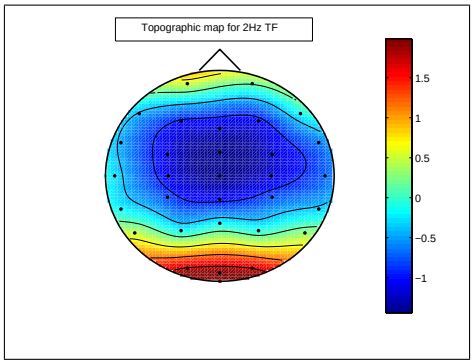

(a) Topograhic map for 2Hz temporal frequency

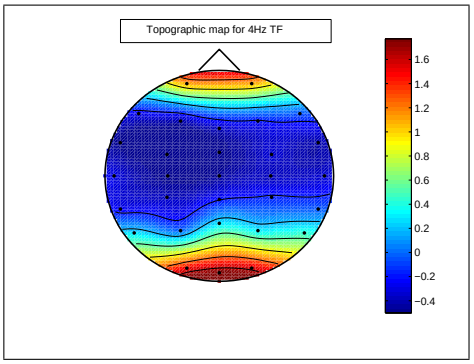

(b) Topograhic map for 4Hz temporal frequency

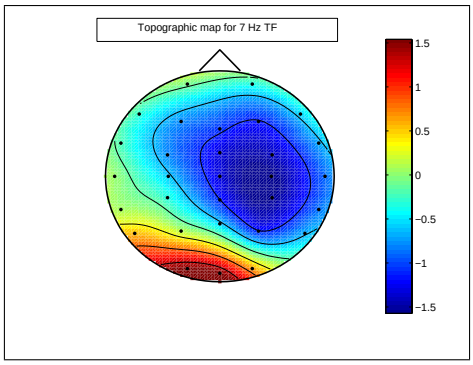

(c) Topograhic map for 7Hz temporal frequency

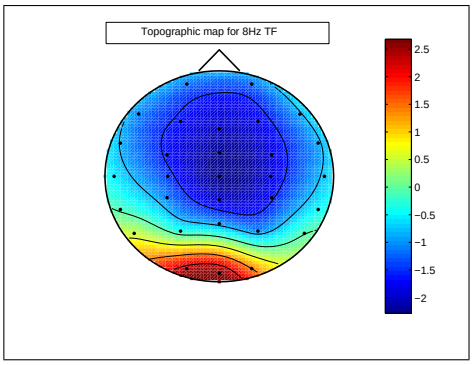

(d) Topograhic map for 8Hz temporal frequency

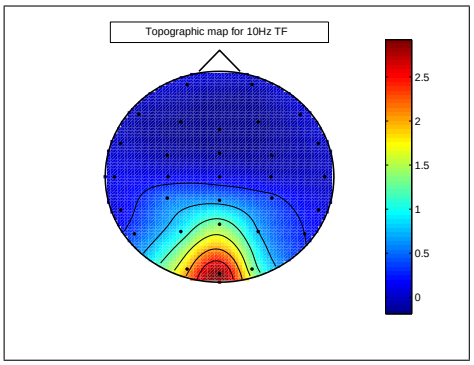

(e) Topograhic map for 10Hz temporal frequency

Figure 3.8 EEG topographic maps

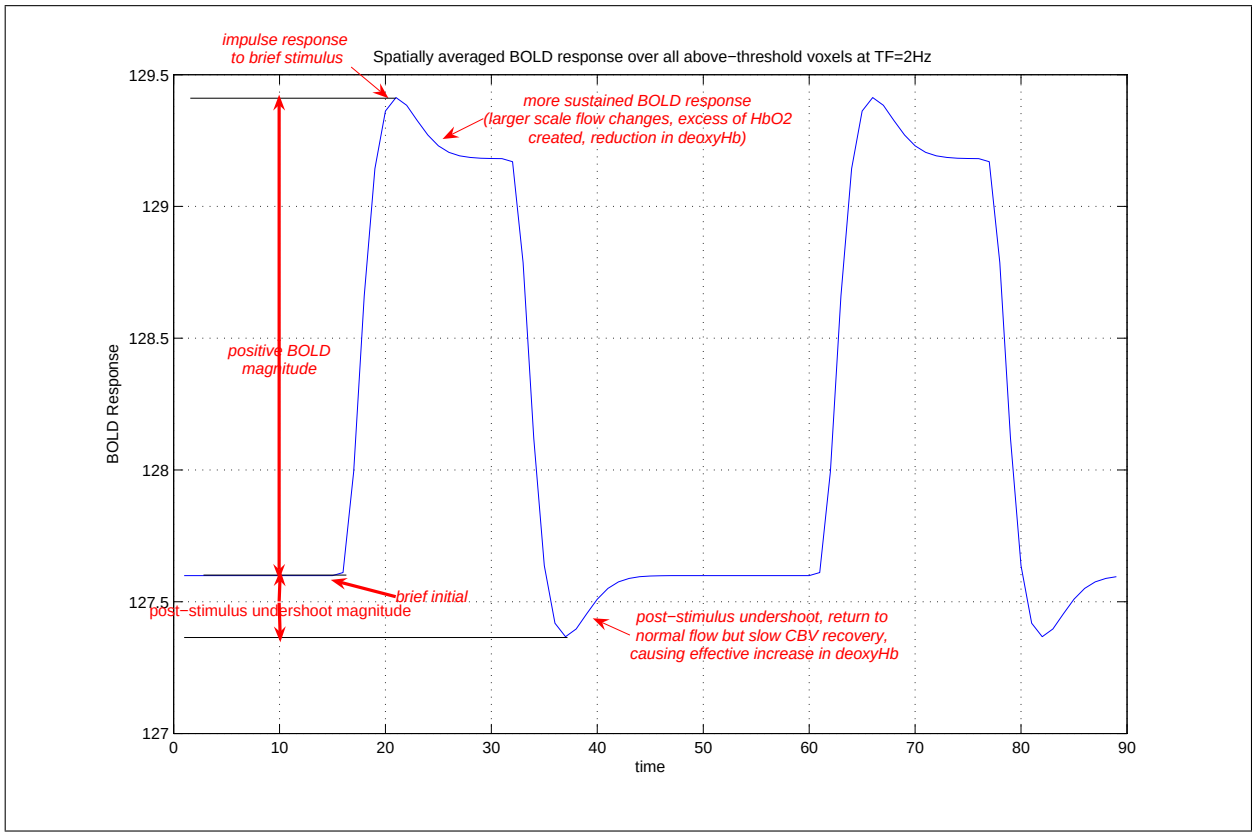

Figure 3.9 At every time instance, the response is averaged over all the supra-threshold voxels and this time-series is constructed. This figure shows the filtered response, i.e, the product of the design matrix and the parameter array of betas. Positive BOLD magnitude and the post-stimulus undershoot is depicted on the graph with red arrows as well as the parts that has physiological outcomes.

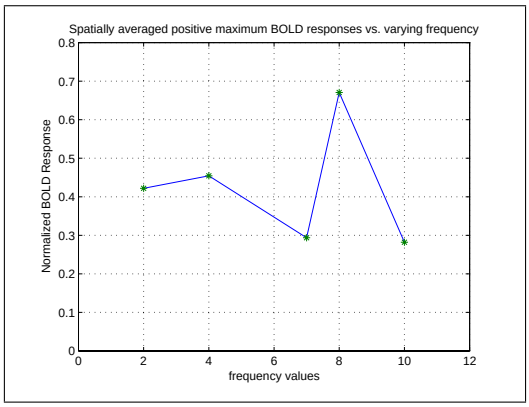

(a) Change in maximum positive BOLD response with respect to temporal frequency

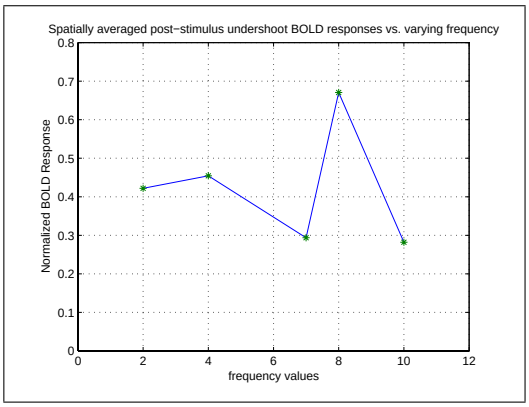

(b) Change in minimum post-stimulus undershoot BOLD response with respect to temporal frequency

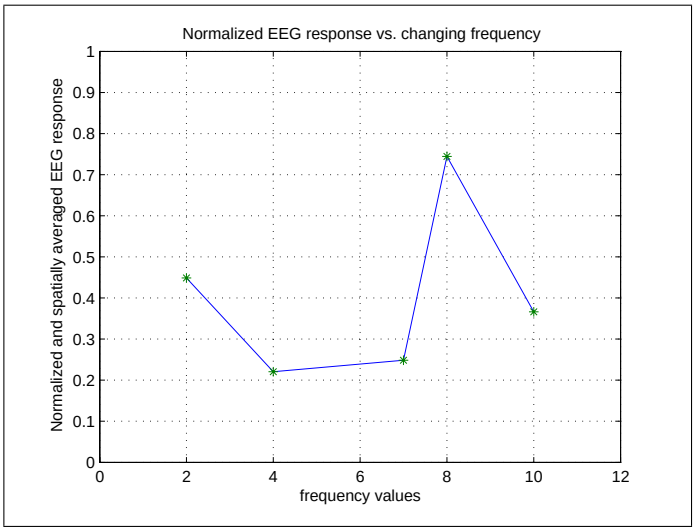

(c) EEG response change with respect to temporal frequency

Figure 3.10 Normalized BOLD-fMRI and EEG response changes vs. stimulus temporal frequencies. fMRI-BOLD response was investigated both for positive maximum signal and the post-stimulus undershoot. Correlation coefficient betweeen the behavior of fMRI and EEG responses is found to be 0.65.

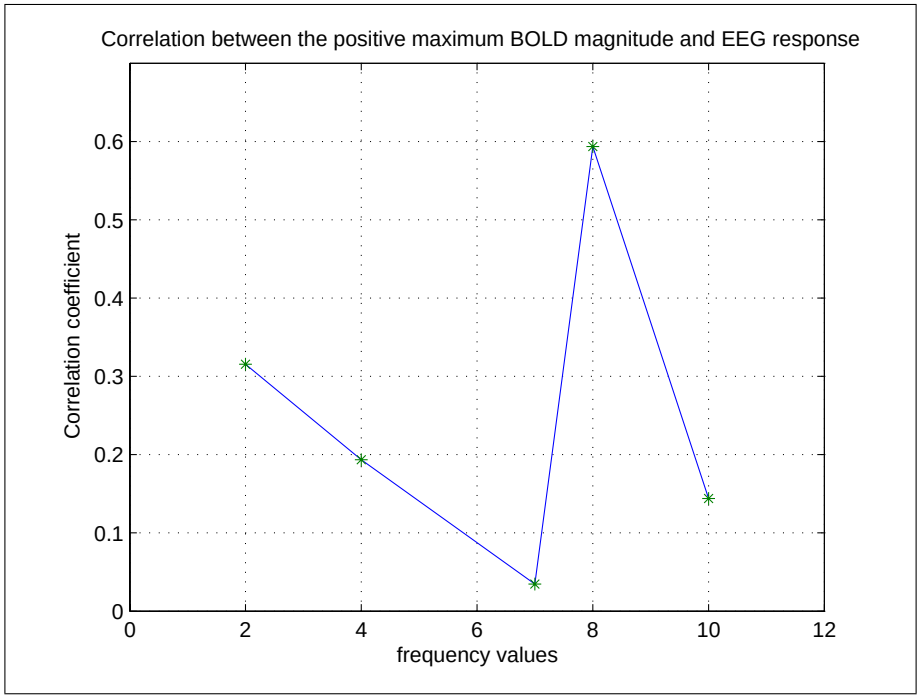

Figure 3.11 Correlation between the positive BOLD response magnitude and the EEG response. These values are taken for each supra-threshold voxel and the correlation coefficient between them are computed for each frequency.

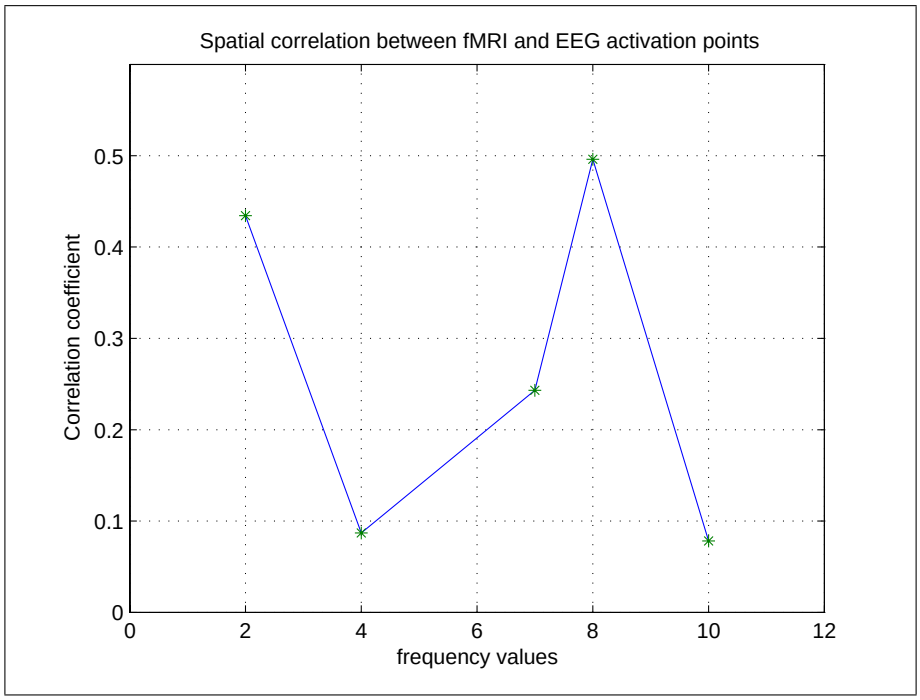

Figure 3.12 Spatial correlation between fMRI and EEG results. Supra-threshold voxels are taken as the correlating sample and fMRI statistical values and LORETA magnitudes are compared.

4. DISCUSSION and CONCLUSIONS

This study investigates the relative changes in the responses of fMRI and EEG with respect to the stimulus frequency. The multi modal analyses performed here revealed important findings about the frequency selective behavior of fMRI response. The results were assessed on a basis of spatial and magnitude correlations.

It is well known that the BOLD signal in fMRI is derived from a combination of stimulus-induced changes in the regional cerebral blood flow (rCBF), local blood volume, and local oxygen consumption rate [38]. The underlying assumption in fMRI is that these changes are due to neuronal activity. There are a number of studies regarding the correlation of the stimulus frequency with this neuronal activity [1]. In these studies, it has been shown that cerebral blood flow is sensitive to the frequency of the stimulus [2].

In a previous study, stimulus rate dependence of regional cerebral blood flow in human striate cortex by positron emission tomography was investigated and the results showed that the rCBF response peaked at 7.8 Hz and then declined [1]. In a different study, rCBF response to frequency variation of pattern-flash visual stimulus was observed and rCBF response in the striate cortex was found to peak at 7 Hz [2]. Also an fMRI study investigated the stimulation frequency dependence of visual activation. The findings agree with the previous positron emission tomography observations and show that the largest MR signal response occurs at 8 Hz [3]. A similar result is found in some research, where it was showed that the fMRI signal also peaks at a flicker frequency of 8 Hz [4]. In another fMRI study, it was found that the BOLD signal change increases up to a stimulus frequency of 6 Hz and then stays nearly constant [5]. Also a recent study revealed that BOLD signal response is also sensitive to spatial frequency variations as well as the temporal frequency changes. In the same study, 8 Hz was the temporal frequency value where the BOLD signal peaked [6].

Our findings support the results of the previous studies. Firstly, in fMRI analysis, the activation was focused on the visual cortex as expected. Visual system responds well to this pure visual stimulus. For some of the frequencies, we also observed mere activation of frontal eye fields and temporal cortex. As for the frequency analysis, BOLD signal changes were observed on the basis of temporal frequency alterations. It was seen that BOLD response increased to the maximum value at 8 Hz. After this, it sharply decreased. This is also consistent with the previous findings. LORETA based EEG source reconstruction results are compatible with fMRI results as well. In addition to the visual cortex activation, EEG response also shows a clear peak at 8 Hz.

LORETA inverse solutions showed the visual cortex activation pretty well for all frequencies and strongly for two and four Hz stimulus frequency. Also in terms of the EEG potential distributions, highlights were observed on the occipital and the frontal cortex. For the low frequencies the distribution is wider whereas as it gets higher, the topography is found to be more focal.

The BOLD responses averaged over the supra-threshold regions are also investigated. The fMRI statistical map voxels which appeared to be active are correlated to the associated EEG amplitudes, which were determined on the same geometric head with LORETA. Spatially averaged positive BOLD, post-stimulus undershoot and LORETA amplitudes are determined across different frequencies. Results from both modalities show us that all of the responses peaked at 8 Hz frequency. For the 2-10 Hz range, the correlation coefficient was found to be 0.65 between positive BOLD response and EEG amplitude behavior. Also, except for the 4 and 7 Hz values, the charactestics showed similar behavior. Spatial correlations are also observed between the positive BOLD and LORETA amplitudes over an activation mask. In this analysis the highest correlation is found at 8 Hz making a sharp change at this point. Different from response effects, the correlation between the standardized regression parameter due to the visual effect and the LORETA amplitudes were also computed over the frequencies. For 2 and 8 Hz, we observed relatively high spatial correlation than the other temporal frequencies. The fact that LORETA makes an assumption initially might have an effect on the results and prevent us from having a higher spatial correlation. In overall, the

most consistent observation for all these analyses is the significant activation increase at 8 Hz as well as the consistent responses taken at this frequency together with a strong correlation between two imaging modalities i.e. the fMRI and EEG. Besides, it is difficult to determine the microvasculature precisely where the BOLD signal originates, because it spreads out into the arteries and these veins can be some distance away from the original location. The fact that fMRI is more sensitive to the arteries might effect our results in terms of the spatial correlations we evaluated.

On the results of this visual stimulation experimental study, we can infer that there is significant correlation between EEG and BOLD signals as a function of changes in the stimulus frequency from 2-10 Hz range. Cortical EEG signals arise mainly in the 50-250 ms range, whereas the BOLD signal arises in the 1-10 sec range. Therefore, the observed findings are not as certain as with the argument that the BOLD signal is linearly related to the time-integrated electrical activity of neurons. This might be due to the fact that the measurements are not sensitive to transient changes in the time series especially in fMRI.

Frequency effect analysis has been a very useful study and it is important in terms of the results it revealed. This study can be broadened in terms of the experimental design and the analysis method. A spatio-temporal analysis could produce more efficient results for analysis. For example, spatial frequency alterations of the visual stimulus may have an important role in the EEG and BOLD responses. The experiment design can be modified in this way and results can be investigated for both of the frequency type changes. Also for comparison purposes, a different protocol for EEG can be proposed. Statistical approach might produce satisfactory results in terms of constructing a common base for EEG and fMRI. Another alternative is considered to replace or modify General Linear Model for EEG. If EEG is provided with its own basis functions, then the model can be improved and results could be presented on a comparative basis.

REFERENCES

1. Fox, P. T., and M. E. Raichle, "Stimulus rate dependence of regional cerebral blood flow in human striate cortex, demonstrated by positron emission tomography," *Journal of Neurophysiology*, Vol. 51, pp. 1109–1120, 1984.

2. Mentis, M. J., G. E. Alexander, C. L. Grady, B. Horwitz, J. Krasuski, P. Pietrini, T. Strassburger, H. Hampel, M. B. Schapiro, and S. I. Rapoport, "Frequency variation of a pattern-flash visual stimulus during pet differentially activates brain from striate through frontal cortex," *NeuroImage*, Vol. 5, pp. 116–128, 1997.

3. Kwong, K. K., J. W. Belliveau, D. A. Chesler, I. E. Goldberg, R. M. Weisskoff, B. P. Poncelet, D. N. Kennedy, B. E. Hoppel, M. S. Cohen, R. Turner, H. Cheng, T. J. Brady, and B. R. Rosen, "Dynamic magnetic resonance imaging of human brain activity during primary sensory stimulation," *National Academy of Sciences*, Vol. 89, pp. 5675–5679, 1992.

4. Thomas, C. G., and R. S. Menon, "Amplitude response and stimulus presentation frequency response of human primary visual cortex using bold epi at 4 t," *Magnetic Resonance in Medicine*, Vol. 40(2), pp. 203–209, 1998.

5. Ozus, B., H. L. Liu, L. Chen, M. B. Iyer, P. T. Fox, and J. H. Gao, "Rate dependence of human visual cortical response due to brief stimulation: an event-related fmri study," *Magnetic Resonance Imaging*, Vol. 19(1), pp. 21–25, 2001.

6. Mirzajani, A., N. Riyahi-Alam, M. A. Oghabian, H. Saberi, and K. Firouznia, "Spatial frequency modulates visual cortical response to temporal frequency variation of visual stimuli: an fmri study," *Physiological Measurement*, Vol. 28, pp. 547–554, 2007.

7. Pascual-Marqui, R. D., C. M. Michel, and D. Lehmann, "Low resolution electromagnetic tomography: a new method for localizing electrical activity in the brain.," *International Journal of Psychophysiology*, Vol. 18(1), pp. 49–65, 1994.

8. "Spm - statistical parametric mapping http://www.fil.ion.ucl.ac.uk/spm/."

9. Clare, S., *Functional Magnetic Resonance Imaging: Methods and Applications*. PhD thesis, University of Nottingham, United Kingdom, 1997.

10. Bandettini, P. A., and L. G. Ungerleider, "From neuron to bold: new connections," *News and Views*, pp. 864–866, 2001.

11. Arthurs, O. J., and S. Boniface, "How well do we understand the neural origins of the fmri bold signal?," *TRENDS in Neurosciences*, Vol. 25, pp. 27–31, 2002.

12. Dale, A. M., "Optimal experimental design for event-related fmri," *Human Brain Mapping*, Vol. 8, pp. 109 – 114, 1999.

13. Henson, R., *Analysis of fMRI time series*, 2003.

14. Friston, K. J., *Experimental Design and Statistical Parametric Mapping*, 2003.

15. Henson, R., C. Büchel, O. Josephs, and K. Friston, "The slice-timing problem in event-related fmri," *NeuroImage*, Vol. 9, p. 125, 1999.

16. Friston, K. J., P. Fletcher, O. Josephs, and A. P. Holmes, "Event-related fmri: characterizing differential responses.," *NeuroImage*, Vol. 7, pp. 30–40, 1998.

17. Friston, K. J., J. Ashburner, C. D. Frith, J. B. Poline, J. D. Heather, and R. S. J. Frackowiak, "Spatial registration and normalization of images," *Human Brain Mapping*, Vol. 3, pp. 165 – 189, 1995.

18. Bosch, J. B., P. S. Valdes, T. A. Virues, V. E. Aubert, E. R. John, T. Harmony, J. R. Diaz, and N. T. Barreto, "3d statistical parametric mapping of eeg source spectra by means of variable resolution electromagnetic tomography (vareta).," *Consciousness and Cognition*, Vol. 32(2), pp. 47–61, 2001.

19. Park, H. J., J. S. Kwon, T. Youn, J. S. Pae, J. J. Kim, M. S. Kim, and K. S. Ha, "Statistical parametric mapping of loreta using high density eeg and individual mri: Application to mismatch negativities in schizophrenia," *Human Brain Mapping*, Vol. 17, pp. 168 – 178, 2002.

20. Barnes, G. R., and A. Hillebrand, "Statistical flattening of meg beamformer images," *Human Brain Mapping*, Vol. 18, pp. 1 – 12, 2003.

21. Kiebel, S. J., and K. J. Friston, "Statistical parametric mapping for event-related potential: I. generic considerations," *NeuroImage*, Vol. 22, pp. 492–502, 2004.

22. Penny, W. D., and K. J. Friston, "Mixtures of general linear models for functional neuroimaging," *IEEE Transactions on Medical Imaging*, Vol. 22(4), pp. 504–514, 2003.

23. Friston, K. J., A. P. Holmes, K. J. Worsley, J. B. Poline, C. Frith, and R. S. J. Frackowiak, "Statistical parametric maps in functional imaging: A general linear approach," *Human Brain Mapping*, Vol. 2, pp. 189–210, 1995.

24. Bandettini, P. A., A. Jesmanowicz, E. C. Wong, and J. S. Hyde, "Processing strategies for time-course data sets in functional mri of the human brain," *Magneetic Resonance in Medicine*, Vol. 30(2), pp. 161–173, 1993.

25. Friston, K. J., P. Jezzard, and R. Turner, "Analysis of functional mri time-series," *Human Brain Mapping*, Vol. 1, pp. 153 – 171, 1994.

26. Aguirre, G. K., E. Zarahn, and M. Desposito, "The variability of human, bold haemodynamic responses," *NeuroImage*, Vol. 8, pp. 360–369, 1998.

27. Buxton, R. B., and L. R. Frank, "A model for the coupling between cerebral blood flow and oxygen metabolism during neural stimulation," *Cerebral Blood Flow and Metabolism*, Vol. 17(1), pp. 64–72, 1997.

28. Josephs, O., R. Turner, and K. Friston, "Event-related fmri," *Human Brain Mapping*, Vol. 5, pp. 243 – 248, 1997.

29. Buckner, R. L., "Event-related fmri and the hemodynamic response," *Human Brain Mapping*, Vol. 6, pp. 373 – 377, 1998.

30. Kiebel, S. J., J. B. Poline, K. J. Friston, A. P. Holmes, and K. J. Worsley, "Robust smoothness estimation in statistical parametric maps using standardized residuals from the general linear model," *NeuroImage*, Vol. 10(6), pp. 756–766, 1999.

31. Kiebel, S. J., and K. J. Friston, "Statistical parametric mapping for event-related potentials i: Generic considerations," *NeuroImage*, Vol. 22, no. 2, pp. 492–502, 2004.

32. Brett, M., W. D. Penny, and S. J. Kiebel, *Human Brain Function, Introduction to Random field theory*, ACADEMIC PRESS, 2003.

33. Kiebel, S. J., J. B. Poline, K. J. Friston, A. P. Holmes, and K. J. Worsley, "Robust smoothness estimation in statistical parametric maps using standardized residuals from the general linear model," *NeuroImage*, Vol. 10, pp. 756–766, 1999.

34. Poline, J. B., K. J. Worsley, A. P. Holmes, R. S. Frackowiak, and K. J. Friston, "Estimating smoothness in statistical parametric maps: variability of p values," *Computer Assisted Tomography*, Vol. 19(5), pp. 788–796, 1995.

35. Worsley, K. J., "Local maxima and the expected euler characteristic of excursion sets of χ^2, f and t fields," *Advances in Applied Probability*, Vol. 26, pp. 13–42, 1994.

36. Poline, J. B., A. P. Holmes, K. J. Worsley, and K. J. Friston, *Making statistical inferences*, Academic Press, 1997.

37. Worsley, K. J., J. E. Taylor, F. Tomaiuolo, and J. Lerch, "Unified univariate and multivariate random field theory," *NeuroImage*, Vol. 23, pp. 189–195, 2004.

38. Ogawa, S., T. M. Lee, A. R. Kay, and D. W. Tank, "Brain magnetic resonance imaging with contrast dependent on blood oxygenation," *National Acad Sciences*, Vol. 87, pp. 9868–9872, 1990.